IDENTIFICATION OF PORE TYPE AND ORIGIN IN A LOWER CRETACEOUS CARBONATE RESERVOIR USING NMR T_2 RELAXATION TIMES

A Thesis

by

DOMENICO LODOLA

Submitted to the Office of Graduate Studies of
Texas A&M University
in partial fulfillment of the requirements for the degree of

MASTER OF SCIENCE

May 2004

Major Subject: Geology

IDENTIFICATION OF PORE TYPE AND ORIGIN IN A LOWER CRETACEOUS CARBONATE RESERVOIR USING NMR T2 RELAXATION TIMES

A Thesis

by

DOMENICO LODOLA

Submitted to Texas A&M University
in partial fulfillment of the requirements
for the degree of

MASTER OF SCIENCE

Approved as to style and content by:

Wayne M. Ahr (Chair of Committee)	Brian J. Willis (Member)
Jerry L. Jensen (Member)	Richard L. Carlson (Head of Department)

May 2004

Major Subject: Geology

ABSTRACT

Identification of Pore Type and Origin in a Lower Cretaceous Carbonate Reservoir
Using NMR T_2 Relaxation Times. (May 2004)
Domenico Lodola, D.E.A., Université Joseph Fourier, Grenoble I (France).
Chair of Advisory Committee: Prof. Wayne M. Ahr

Determining the distribution of porosity and permeability is one of the main challenges in carbonate petroleum reservoir characterization and requires a thorough understanding of pore type and origin, as well as their spatial distributions. Conventional studies of carbonate reservoirs require interpretation and analysis of cores to understand porosity. This study investigates the use of NMR logs in the determination of pore type and origin.

This study is based on the analysis of both thin section petrographic and NMR data from a single well that cored the Lower Cretaceous (Aptian) shelf carbonates belonging to the Shuaiba Formation of the Middle East. Photographs of thin sections were used to determine pore type and origin according to Ahr's genetic classification of carbonate porosity. Descriptive statistics and modeling were used to analyze the NMR T_2 relaxation time distributions. Descriptive statistical analyses included estimating arithmetic average, standard deviation, skewness, median, mode and 90th percentile. T_2 modeling was performed by fitting multiple log-normal distributions to the measured T_2 distribution. Data from thin section petrography and from NMR measurements were then compared using conditional probabilities.

As expected, thin section analysis revealed the predominance of mud-supported fabrics and micropores between matrix grains Vugs and dissolved rudistid fragments account for most of the macro porosity. Descriptive statistics showed that the mode and

90^{th} percentile of the T_2 distribution had the greatest power to discriminate pores by origin. The first principal component (PC1) of the mode-90^{th} percentile system was then used to compute the probabilities of having each pore origin, knowing that PC1 belongs to a given interval. Results were good, with each origin being predictable within a certain range of PC1.

Decomposition of the T_2 distributions was performed using up to 3 log-normal component distributions. Samples of different pore origin behaved distinctively. Depositional porosity showed no increase in fit quality with increasing number of distributions whereas facies selective and diagenetic porosity did, with diagenetic porosity showing the greatest increase.

ACKNOWLEDGEMENTS

First and foremost, I wish to thank Wayne Ahr for his support and advising throughout my stay at Texas A&M. He helped me not only during this research project, but all the way from before day one, including the lengthy application process to the University. His trust and enthusiasm was a constant motivation during ongoing work.

I wish to thank Jerry Jensen and Brian Willis for agreeing to be members of my advisory committee. Jerry Jensen provided valuable information and comments on the statistics that were used in this work. Brian Willis provided excellent proof-reading of my draft and insightful comments on my work. I would like to extend my gratitude to Richard Carlson and the staff of the Department of Geology & Geophysics for welcoming me into their department and for the help they provided.

I would also like to express my deepest appreciation towards Schlumberger, who provided both the data for this work and the funding for my studies at Texas A&M and the IFP-School. In particular, I wish to thank Isabelle Lenir, David Allen and Emmanuel Bize for offering me this opportunity and setting up my thesis project.

I would also like to thank Alain Auriault and the staff at the IFP-School for their support and advising.

Finally, special thanks go to Ahmed Mabrouk, who not only helped me out on too numerous occasions, but who also proved to be a good friend.

TABLE OF CONTENTS

Page

LIST OF FIGURES

LIST OF TABLES

INTRODUCTION

Determining the distribution of porosity and permeability is one of the main challenges in carbonate petroleum reservoir characterization. Porosity is influenced by a variety of depositional and diagenetic processes that can produce different pore-types (e.g., intergranular, moldic, vuggy). Permeability is linked to pore type by such parameters as pore-to-pore-throat ratio and coordination number, which are both functions of pore type.

An understanding of processes that produce porosity and the spatial distribution of reservoir qualities can be achieved from the study of cored sections and outcrop equivalents. Conventional logs are however typically of little use in this domain because of the relative complexity of carbonate porosity. The proposed study will investigate the use of NMR logs in the determination of pore type and origin.

Although core images have been used before for the calibration of NMR data (e.g. Ausbrooks *et al*., 1999), there are few published studies of the relationships between pore shape/type and NMR response. NMR data are usually used as a method of determining porosity and permeability, and in general, independently of pore characteristics.

The objective of this study is to identify relationships between pore characteristics and NMR data. To reach this objective, pore type and origin data gathered from thin section photographs will be compared to statistical analysis and modeling of the NMR data. Conditional probabilities will be applied to these results to identify the best relationships.

This thesis follows the style and format of the American Association of Petroleum Geologists Bulletin.

NMR BASICS

We review here the basic physics and interpretation of NMR measurements. The presentation follows that of Coates *et al*. (1999).

NMR PHYSICS

Nuclear magnetic resonance (NMR) may be summarized as the response of certain nuclei to a magnetic field. Not all nuclei in nature are affected by NMR, as it only affects nuclei that have either an odd number of protons, or neutrons or both. Hydrogen is a element that meets these requirements (it only has a single proton) and is very abundant in pore fluids (water, oil and gas).

Static fields and polarization

Protons spinning on themselves create a current loop that induces a bipolar magnetic field. When subjected to a static magnetic field B_0, the magnetic bipole of a hydrogen nucleus will align and precess around B_0 at a given frequency called the Larmor frequency. Different elements will have different Larmor frequencies. If only hydrogen nuclei are considered, then the Larmor frequency is solely determined by the strength of the magnetic field. As B_0 varies in space, the spatial region investigated by a NMR tool can be chosen by adjusting the Larmor frequency.

When the protons align with the static field, they align either in a parallel way (known as low-energy state) or an anti-parallel way (known as high-energy state). However more protons precess in a low energy state. The resulting difference in the number of parallel and anti-parallel protons is known as bulk magnetization M_0 and can be measured by NMR tools.

Nucleus polarization is not an instantaneous process. It is instead a progressive

phenomenon and magnitude of polarization $M_z(t)$ exponentially increases with time:

$$M_z(t) = M_0\left(1 - e^{\frac{-t}{T_1}}\right) \quad \text{..... (1)}$$

where

M_0 = final and maximum magnetization
t = exposure time to B_0 field
T_1 = longitudinal relaxation time

T_1 is called longitudinal relaxation time as it controls longitudinal (parallel to B_0) magnetization time. Polarization is reached when all protons are aligned with B_0 and $M_z = M_0$.

Oscillating fields, pulse tipping and spin-echoes

If an oscillating magnetic field B_1 is applied at right-angles to B_0, the magnetization will be tipped and a transverse magnetization can be measured. This tipping is due to changes in proton energy state from low to high (energy absorption) and their in-phase precession around B_0 induced by the oscillating field. These interactions between protons and B_1 are called magnetic resonance. Most effective tipping will occur for B_1 oscillating at the Larmor frequency.

Once the oscillating field stops, protons will diphase due to inhomogeneities in the static field, and transverse magnetization will decay. This decay, called free induction decay (FID) is exponential and is governed by the FID time constant T_2^*.

In a CPMG sequence (named after its inventors, Carr, Purcell, Meiboom and Gill) a 90° pulse (oscillating magnetic pulse at right-angles with B_0) is first applied and results in the creation of a transverse magnetization. As protons start to diphase, 180° pulses are applied after a time τ and then every 2τ. The 180° pulse causes protons to temporarily re-phase and measurable spin-echoes are generated at 2τ, 4τ, 6τ, … The dephasing due

to molecular interactions and diffusion is, however, irreversible and the amplitude of the transverse magnetization M_x decays exponentially with time:

$$M_x(t) = M_{0x} e^{\frac{-t}{T_2}} \quad \text{..... (2)}$$

where

T_2 = transverse relaxation time constant

M_{0x} = initial transverse magnetization

A set of CPMG sequences is characterized by two time values: inter-echo spacing *TE* which is the time between to successive 180° pulses; and polarization time *TW* which is allowed between each individual CPMG sequence. This polarization time is necessary as protons will be randomly orientated after each sequence and a certain time is needed for them to re-polarize prior to further magnetic resonance measurements. The number of echoes *NE* can also be controlled.

Varying these parameters will affect both what is measured and the quality of the measurements. For example, decreasing *TE* will increase the spin-echoes sampling rate and thus increase the signal to noise ratio. Low *TE* will also allow low T_2 times (such as in clay bound water) to be measured. Polarization time is different for each fluid and varying *TW* will act (at least in part) as a filter for fluid type. Light hydrocarbons for example have longer polarization times than water; if pore fluids are present, decreasing *TW* will allow only water to reach complete polarization hence filtering out the hydrocarbons.

Relaxation times

Relaxation times are the results of three mechanisms that act in parallel: bulk relaxation, surface relaxation and diffusion. Total transverse relaxation time can be written:

$$\frac{1}{T_2} = \frac{1}{T_{2bulk}} + \frac{1}{T_{2surface}} + \frac{1}{T_{2diffusion}} \quad \text{..... (3)}$$

where

T_{2bulk} = T_2 relaxation time of pore fluid as it would be measured in an infinite container (no surface effects)

$T_{2surface}$ = T_2 relaxation time of pore fluid resulting from surface relaxation

$T_{2diffusion}$ = T_2 relaxation time of pore fluid induced by diffusion in the magnetic field gradient

Bulk relaxation is an intrinsic relaxation property of a fluid. Bulk relaxation times may be calculated for any given fluid and are function of the fluid's physical properties and temperature.

Surface relaxation corresponds to relaxation induced by interactions between the fluid and the surface of the pore. It is influenced by surface to volume ratio S/V and surface relaxivity ρ_2 which expresses the ability of the surface to induce relaxation. Surface relaxation times are therefore a function of pore geometry and lithology:

$$\frac{1}{T_{2surface}} = \rho_2 \left(\frac{S}{V} \right)_{pore} \quad \text{..... (4)}$$

Typical values of ρ_2 are 15 μm/sec in sandstones and 5 μm/sec in carbonates (Chang *et al.*, 1997). Surface relaxation times are thus longer in carbonates.

Diffusion induced relaxation is the result of de-phasing of protons caused by their diffusion in the fluid. This diffusion occurs when a strong gradient exists in the magnetic field, and protons move between zones where the field strength is different. Diffusion effects may be observed in gas, light to medium-viscosity oils and water, and is strongly influenced by inter-echo spacing *TE*.

The relative importance of each relaxation mechanism varies mainly with fluid composition and acquisition parameters. If only brine is present in pores, then transverse relaxation times are dominated by surface relaxation and hence T_2 can be considered as a direct indicator of pore size:

$$\frac{1}{T_2} = \rho_2\left(\frac{S}{V}\right) \quad \text{..... (5)}$$

If the pores have a spherical shape, T_2 will be proportional to r, the radius of the pore.

Multi-exponential decays

In porous media, NMR encounters different pore sizes and different fluid types. As seen in equations 5 for the case of brine, each pore size will correspond to a single T_2 value and, by extension, the pore-size distribution to a T_2 distribution. Transverse magnetization will no longer decay with a unique T_2 value, but as a multi-exponential function corresponding to this T_2 distribution. Equation 2 can thus be re-written as the sum of multiple exponential decays:

$$M(t) = \sum_i M_{0i} e^{\frac{t}{T_{2i}}} \quad \text{..... (6)}$$

where i represents the ith component of pore size and T_{2i} its corresponding T_2.

By mathematical inversion techniques, the multi-exponential decay measured with a CPMG sequence can be transformed into the corresponding T_2 distribution. Although a continuous function, this T_2 distribution is in practice discretized into a finite number of pre-selected T_2 values known as T_2 bins. The resulting distribution is a T_2 versus incremental porosity curve.

CONVENTIONAL NMR INTERPRETATION

Porosity

Porosity is the simplest petrophysical parameter to estimate with NMR. Initial magnetization of the spin echo curve – which is equal to the area under the T_2 distribution curve, is proportional to the total number of hydrogen atoms present in the

pore fluids of the investigated area. Once calibrated to hydrogen atom density in bulk fluid, initial magnetization can be used to measure total porosity. This implies that NMR porosity measurements are independent of lithology.

Unlike conventional logs that require shale corrections, the NMR tool is able to distinguish between "true" porosity and clay bound water if two successive measurements are made. Indeed clay bound water having very low T_2 relaxation times, a first run with a low *TE* will include clay-bound water while a second run with a higher *TE* will not. The second run will thus no longer measure clay bound water and will only measure true pore space.

Permeability

A necessary step in estimating permeability is determining which part of porosity is actively controlling permeability. Two methods have been put forth in the literature for NMR data. The first method assumes that permeability is controlled by the geometric mean of the T_2 distribution, and is generally know as the SDR method (Schlumberger Doll Research). Chang *et al.* (1994) studied vuggy dolomites and suggested a relationship between permeability, porosity and T_2 geometric mean:

$$k = a\phi^4 T_{2GM}^2 \quad \text{.....(7)}$$

Where T_{2GM} is the geometric mean of the T_2 distribution and a is a correlating factor. Their study yielded a value of 4.75 for a (after a T_2 cut-off at 750ms was applied to account for the unconnected vuggy porosity). In a study of 64 carbonate plugs belonging to two oil fields, Lyne *et al.* (1996) proposed a variation of the SDR model where A, B and C are to be calibrated with core permeability data:

$$k = A \cdot \phi^B \cdot T_{2GM}^C \quad \text{.....(8)}$$

The second method, known as the Timur-Coates model, uses the ratio of free fluid ($FFI = \phi - BVI$) to bulk volume of irreducible water (*BVI*) as an estimation of porosity contributing to fluid flow (Coates, 1999):

$$k = \left[\left(\frac{\phi}{C}\right)^2\left(\frac{FFI}{BVI}\right)\right]^2 \quad \text{..... (9)}$$

C is a correlation constant and needs to be calibrated using other permeability data. Logan *et al*. (1998) noted that this model relies on a T_2 cut-off value to determine free-fluids. The correct cut-off value is difficult to determine in carbonates and hence the SDR method should be preferred for use in carbonates.

Both these techniques are based on the direct link between T_2 values and pore-size – and by extension to pore-throat size, to estimate permeability. This is acceptable in simple geometries like stacking of spherical grains. It may not however be as true in the more complicated pore geometries that are observed in carbonates.

DATA ORIGIN AND ACQUISITION

The data used for this study come from a single cored well of the Shuaiba Formation (Lower Cretaceous) in the Middle East (approximately 650 feet thick). Plugs were taken from this core at 65 different depths and these were used to make thin sections, perform conventional core analysis and measure NMR T_2 relaxation times. All these data are available at same depths.

THE SHUAIBA FORMATION

The Aptian Shuaiba Formation is composed of thick porous shelf carbonates with considerable subsurface lateral and vertical lithofacies variations over much of the Arabian platform (Alsharhan *et al.*, 2000). The Shuaiba Formation is informally subdivided into two members, the Lower Member and the Upper Member. The Lower Member is known as Thanama I, Thanama A or Thanama IA. It is composed mainly of wackestones and packstones overlain by microporous lime mudstone at its base; and medium-grained wackestones and boundstones at its top. The Upper Member is composed of mostly medium- to coarse-grained packstones and grainstones and is characterized by abundant rudistid fragments.

A diagenetic study of the Shuaiba Formation of the Ghaba North Field in Oman (al-Awar and Humphrey, 2000) shows that most porosity is due to microporosity (up to 95%) with macroporosity increasing towards the top of the formation. This microporosity accounts for most of the hydrocarbon storage capacity and corresponds to the micro-rhombic calcite matrix. Macroporosity is mainly found in partially or completely dissolved rudistid fragments. Macroscopic calcite cements are rare due to the lack of interparticle macropore space resulting from the predominance of mud-supported fabrics.

Russell *et al.* (2002) identified 17 reservoir rock types in the Shuaiba Formation of the U.A.E. Porosities range from less than 5% to 30% and permeabilities from 0.01mD to over 1D.

AVAILABLE DATA

Thin section photographs

Detailed photographs of the full thin sections were available for this study. The thin sections were made with blue resin to help identify porosity. All photographs were taken at the same scale allowing comparisons between different samples.

Conventional core analysis

Porosity

Schlumberger Doll Research made porosity measurements on both 1.5" diameter by 1.5" long and 0.75" diameter by 1.5" long plugs. The plugs were dried in a vacuum oven at 105°C for 12 hours. The plug samples were then allowed to equilibrate to room temperature in a desiccator. Each plug was transferred to a Micromeritics AccuPyc 1330 pycnometer and the grain volume was measured according to Boyle's law (gas expansion). Calipers were used to measure the length and diameters of the plugs and these measurements were used to calculate bulk volume. The porosity is the difference between the bulk and grain volumes.

Permeability

Schlumberger Doll Research also collected permeability measurements on the same plugs as porosity. Permeability measurements were made using an automated gas permeameter developed at Schlumberger-Doll Research. The instrument was designed to measure permeabilities of porous samples ranging from 0.1 mD to 10 D within 0.5%. The core plug was evacuated and dried in a vacuum oven prior to the permeability

measurement. The core was mounted in the permeability apparatus and surrounded by a rubber sleeve to which a pressure of 80 psi was applied to seal the outer surface of the core. Nitrogen gas was flowed through the core and pressure and flow rates were measured. An algorithm uses the measurements to calculate the permeability of the core.

NMR

NMR experiments were performed in Schlumberger Doll Research's NMR Laboratory using a MARAN low field (2 MHz) hydrogen magnetic resonance instrument. The T_2 distributions were computed by evaluating the Carr-Purcell-Meiboom-Gill (CPMG) measurements. The inter-echo spacing used in these experiments was 600 μsec and the delay time was 10 seconds. The NMR of a standard sample was collected each day to ensure quality control and as a means of calculating the fluid volume based on the amplitude of the calibration standard NMR signal. The NMR of the fully brine saturated samples was measured first. The samples were then centrifuged at about 25 psi vs. air for 24 hours and the NMR of the partially saturated plugs was measured. Next, the samples were centrifuged at about 100 psi vs. air for 24 hours and the NMR distribution of the partially saturated plugs was measured.

METHODS

In order to find relationships between NMR curve shape and pore characteristics, both NMR T_2 distributions and photographs of thin sections were independently studied. Thin section photograph interpretation were used to define reference pore characteristics that are compared to various statistical measures of the NMR data.

THIN SECTION PHOTOGRAPH INTERPRETATION

Three main characteristics were determined from thin-section photographs. First, samples were classified according to a simplified version of Dunham's classification of carbonate rocks (mudstone, wackestone, packstone and grainstone). This provides a general idea of grain size and arrangement and a first order classification of pore characteristics.

Second, pore-types (e.g.: matrix, intergranular, vuggy, moldic) will be identified and described for each sample and their relative abundances will be estimated. In view of the objectives of this study, general trends in pore characteristics are sought and thus abundances will be estimated on a deliberately simple scale (present, abundant, very abundant). To some extent size and shape of pores can be inferred by pore-type.

Finally each sample has been classified according to Ahr's genetic classification of carbonate porosity (Ahr, 1999; Figure 1) and each sample was given a unique pore origin. This genetic classification provides a synthetic view of pore characteristics, from simple depositional porosity to complex diagenetic porosity with multiple pore types.

Thin section photographs are not the optimum data source for this type of classification, as they are limited in resolution when compared to the original thin sections. However they produce an equivalent "image" of the rock and provide a pore-type identifying tool comparable to the thin sections used in most studies. They are also

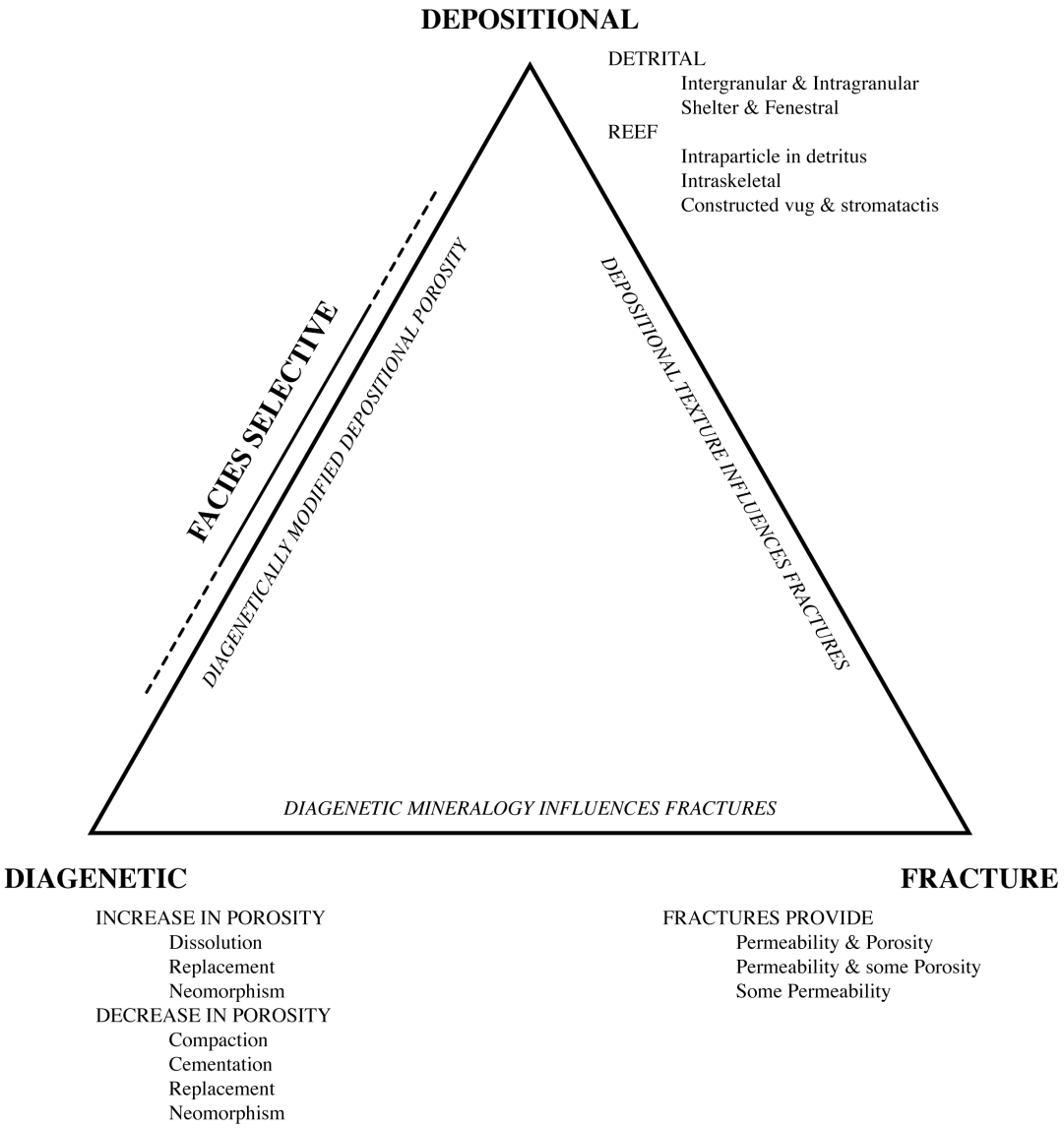

Figure 1. Genetic classification of carbonate porosity (modified from Ahr, 1999).

affected by the same limitations. Amongst these limitations are representativeness of the sample, relationship between 2D view of the pore provided by the photograph and true 3D shape of pores, difficulties identifying small pores like matrix porosity, and difficulties in correctly estimating proportions of large pores.

For each sample, thin section interpretation provides a unique pore origin and a series of pore types.

NMR CURVE ANALYSIS

T_2 distribution shapes (NMR curves) were analyzed in two different ways. First, general shape and trend of the curves are described using descriptive statistics. Second, distributions are modeled by fitting multiple unimodal distributions to the measured data.

Descriptive statistics

The first parameters calculated were the arithmetic average and sample variance. Due to the discrete nature of NMR data, true population mean and variance of the T_2 distribution could not be measured. Instead only the sample mean and variance were calculated. The difference between sample and population were small due to the high sampling rate. Mean and variance are estimated as follows:

$$\overline{T_2} = \frac{\sum T_{2,i} \cdot A_i}{\sum A_i} \quad \text{..... (10)}$$

$$Var(T_2) = \frac{\sum A_i \left(T_{2,i} - \overline{T_2}\right)^2}{\sum A_i} \quad \text{..... (11)}$$

where

$T_{2,i}$ = T_2 bin

A_i = amplitude of the ith T_2 bin

These are standard parameters used to describe a given distribution and describe the general shape of curve. The average approximates the expected value of the T_2 distribution and, by extension, the expected "pore-size". The variance indicates how much variability exists in the data around this expected value: extent to which the data are well grouped around this central value or will it be spread out.

To further describe the shape of the T_2 distribution, the sample median and 90th percentile were calculated. The median and the 90th percentile are taken directly from the sample cumulative density functions as the first T_2 bin to account respectively for 50% and 90% of the cumulative porosity. The 90th percentile indicates the behavior of the distribution towards high T_2 values (cutoff or stretching). It helps identify vuggy porosity. The median, when compared to the average, helped characterize the asymmetry of the distribution. Asymmetry of the distribution was further investigated with the coefficient of skewness γ_1:

$$\gamma_1 = \frac{\mu_3'}{\mu_2'} = \frac{\sum A_i \left(T_{2,i} - \overline{T_2}\right)^3 \Big/ \sum A_i}{Var\left(T_2\right)^{1.5}} \quad \text{..... (12)}$$

Skewness is a function of the third centered moment and quantifies the asymmetry of a distribution. A positive γ_1 corresponds to a distribution stretched towards the higher T_2 values and a negative γ_1 reflects a distribution stretched towards the lower T_2 values.

The mode was calculated by taking the T_2 bin with the highest amplitude. In the case of multi-modal distributions, only the mode with the greatest amplitude was retained. This maintains consistency of interpretation throughout the data set and provided a single mode value for each sample. The mode measures the most abundant pore-size.

Finally, arithmetic average and variance of all statistical parameters as well as variance-covariance and correlation matrices were calculated as follows:

$$\overline{X} = \frac{\sum X_i}{N} \quad \text{..... (13)}$$

$$Var(X) = \frac{\sum\left(X_i - \overline{X}\right)^2}{N-1} \quad \text{..... (14)}$$

$$CoVar(X,Y) = \frac{\sum\left(X_i - \overline{X}\right)\left(Y_i - \overline{Y}\right)}{N-1} \quad \text{..... (15)}$$

$$r = \frac{CoVar(X,Y)}{\sqrt{Var(X)Var(Y)}} \quad \text{..... (16)}$$

where N is the number of samples and X and Y are two parameters. Correlation coefficient r quantifies the correlation between two parameters. If $r = \pm 1$ then X and Y are perfectly correlated (or anti-correlated). If $r = 0$, X and Y typically show no correlation.

T2 distribution modeling

A given T_2 value can be interpreted as a pore-size (Equation 5). In the case of stacked spherical grains, the T_2 value is proportional to r, the radius of the grains. For grain size of a certain distribution, the pore-size will follow a closely linked distribution. This in turn implies that NMR relaxation times will follow a distribution controlled by grain-size distribution.

In the case of carbonate porosity, where multiple pore types are present, each pore type will have its own size distribution. Each of these distributions will translate into individual T_2 distributions controlled by the size of the pores and their surface to volume ratio. Under this hypothesis, the observed T_2 distribution will be the sum of multiple distributions, each corresponding to the size distributions of individual pore types. Identifying these individual distributions reveals information on pore types.

The T_2 distributions were modeled by fitting multiple log-normal distributions to the measured data. Log-normal distributions were initially chosen because NMR curves typically exhibited normal distributions on a semi-log plot. Probability plots can help determine distribution type. Figure 2 shows a normal and a log-normal probability plot

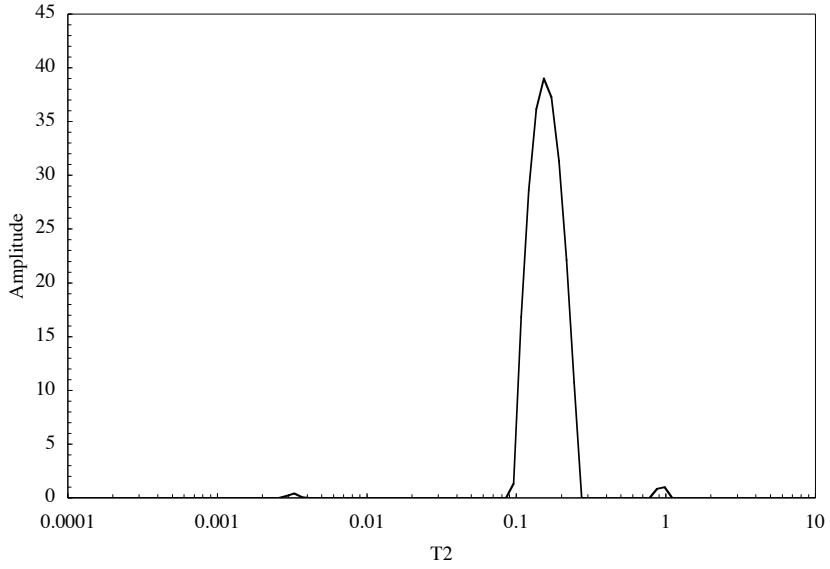

(A)

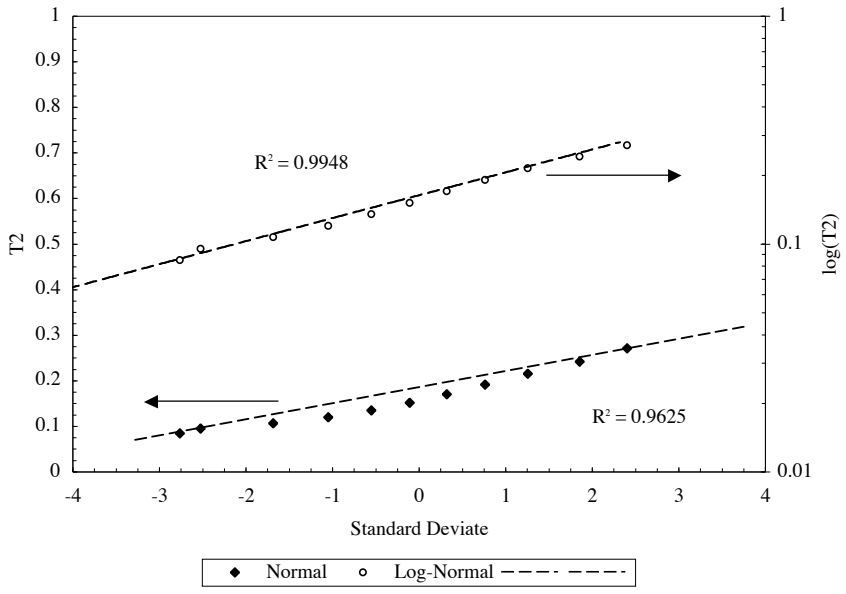

(B)

Figure 2. T_2 distribution at 8727' (A); and corresponding normal and log-normal probability plots (B).

for the sample at depth 8727'. The small variability of the T_2 distribution makes the log-normal and normal distributions indistinguishable. This sample exhibits a unimodal T_2 distribution and plots out as a normal or log-normal distribution equally well.

The multiple log-normal distributions used in this study are the weighted sum of several independent log-normal distributions of given average and variance. They can be described as:

$$f_{model}(T_2) = A\sum \alpha_i \cdot g_i\left(\mu_i,\sigma_i^2,T_2\right) \quad \text{..... (17)}$$

with $\sum \alpha_i = 1$

where:

f_{model} = model distribution

A = amplitude multiplier

$g_i\left(\mu_i,\sigma_i^2,T_2\right)$ = individual log-normal distribution with average μ_i and variance σ_i^2

T_2 = T_2 values for which the model is computed

α_i = proportion of individual log-normal distribution

The amplitude multiplier A accounts for the porosity value of each sample. The T_2 distributions not being normalized, the area under the curves are not equal to 1, but rather to porosity. There should be a linear relationship between porosity and A. The weights are the percentage of total porosity attributed to each individual distribution.

The best fit is obtained by minimizing the sum of squared errors (SSE) using Excel's built-in (non-linear) Solver application. The SSE may be expressed as:

$$SSE = \sum_i \left(f_{observed}(T_{2,i}) - f_{model}(T_{2,i})\right)^2 \quad \text{..... (18)}$$

While the SSE represents a good tool for optimizing the fit of the model, it is a non normalized value and is thus not a good tool for comparing fit quality between different samples. Instead, the coefficient of determination R^2 will be used for comparing the

results between different samples. R^2 is a normalized estimator of the correlation between the observed data and the estimated (modeled) data. It is calculated as follows:

$$R^2 = 1 - \frac{\sum\left(f_{observed}\left(T_{2,i}\right) - f_{model}\left(T_{2,i}\right)\right)^2}{\sum\left(f_{observed}\left(T_{2,i}\right) - \overline{f_{observed}\left(T_2\right)}\right)^2} \quad \text{..... (19)}$$

An example of T_2 modeling with three distributions is shown in Figure 3. Measured data, the total model and its individual log-normal distributions, and the absolute error of the model are shown. Also shown is a cross-plot of measured versus modeled amplitude for each T_2 bin and the corresponding coefficient of determination.

For each sample, the fitting of these log-normal curves will yield a series of averages, standard deviations and weights corresponding to each individual distribution, as well as modeling coefficient, SSE and R^2 values for the complete model.

In order to simplify calculations, the T_2 bins were *log* transformed prior to modeling, and multiple Gaussian distributions were fitted. This corresponds to fitting the $log(T_2)$ distribution using Gaussian component distributions.

COMBINING AND COMPARING DATA FROM DIFFERENT SOURCES

Principal Component Analysis

Once the descriptive statistical parameters have been calculated for the NMR data, the results were analyzed to determine parameters that best identify pore origin. Principal components analysis (PCA) allows us to study multivariate data sets and determine linear combinations of the variables (the principal components) for which variations are greatest.

PCA calculates the eigenvalues and eigenvectors of the variance-covariance matrix of the data (Davis, 1986). If A is a square matrix of dimension n, then the eigenvalues will be the vector with n rows such that:

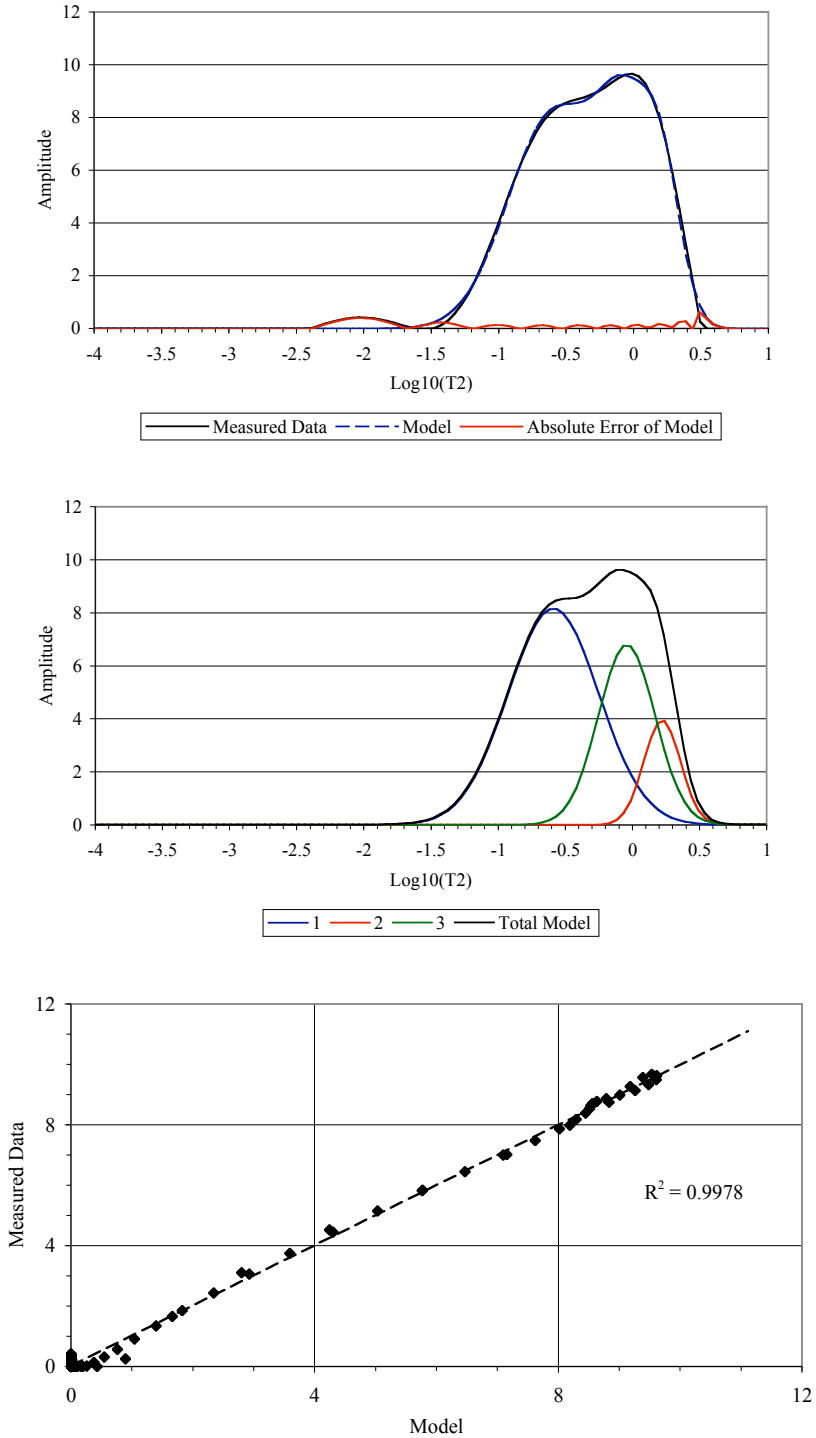

Figure 3. Example of T_2 modeling using three distributions (depth of shown sample: 8132.17').

$$\det\left|A - \lambda I\right| = 0 \quad \text{..... (20)}$$

The i[th] eigenvalue then gives the i[th] eigenvector X_i (corresponding to the i[th] principal component) such that:

$$\left(A - \lambda_i\right) \cdot X_i = 0 \quad \text{..... (21)}$$

Algorithms to calculate both eigenvalues and eigenvectors are preprogrammed on most modern scientific calculators and are thus very easy to obtain.

The eigenvalues give the relative proportion of the total variance represented by each of the principal components. The eigenvectors give linear combinations of variables that make up the principal components. Within a given principal component, the coefficients given by the eigenvector to each variable will indicate the relative contribution of that variable to the total variability of the principal component.

Conditional probabilities and Bayes' theory

When a parameter, or a combination of parameters, was shown by statistical analysis of the NMR data to identify pore origin, conditional probabilities were used to test the accuracy of this measure. The probability $P\left(Q = q_i \mid x \le X < x + h\right)$ was used, as it represents the probability that pore origin (Q) is q_i knowing that a measured statistical parameter (or combination of parameters) X satisfies $x \le X < x + h$. This probability can be determined using Bayes' theorem (Fisz, 1980):

$$P\left(Q = q_i \mid x \le X < x + h\right) = \frac{P\left(Q = q_i\right)P\left(x \le X < x + h \mid Q = q_i\right)}{\sum_j P\left(Q = q_j\right)P\left(x \le X < x + h \mid Q = q_j\right)} \quad \text{..... (22)}$$

The probabilities necessary for the application of Bayes' theorem are easily calculated. $P\left(Q = q_i\right)$ is the ratio of the number of samples where pore origin is q_i divided by the total number of samples. $P\left(x \le X < x + h \mid Q = q_i\right)$ is estimated by the ratio of the number of samples where $x \le X < x + h$ and pore origin is q_i divided by the number of samples where pore origin is q_i.

RESULTS

ROCK AND PORE CHARACTERISTICS

Simplified Dunham classification, pore types present (simplified and modified from Choquette and Pray, 1970) and genetic classification of pore origin resulting from the thin section photograph interpretation are shown in Table 1. Observed pore types are matrix, intergranular, moldic (rectangular and round), matrix dissolution, vuggy and intragranular. Photographs of common pore types are shown in Figure 4.

More coarse-grained samples are present in the upper half of the core (Upper Shuaiba). Packstones and grainstones were dominant at the top, and mudstones and wackestones are dominant towards the bottom (Thanama I). Matrix porosity/microporosity dominates throughout.

Most of the samples are affected by diagenesis to some extent. Very few samples exhibit pure depositional porosity. Rare samples showing depositional pores are fine-grained (mudstones to wackestones).

Moldic pores are present throughout the core, and are usually formed by dissolved rudistid fragments. These molds may either be roundish or rectangular, depending on the shape and size of the original fragment. Rectangular molds are bigger and more common towards the top of the core whereas rounded molds are more common towards the base. This may be due to a greater transport and wearing of fragments deposited at the base of the section.

Two types of intragranular porosity were distinguished: that found in foraminifera (orbitolinids and chrysalinids), and, less frequently, that in partially dissolved rudistid fragments and other grains. Intragranular porosity probably accounts for very little the of total porosity.

Table 1. Pore characteristics determined with thin section photographs.

Depth *feet*	Grain size*	Matrix†	Inter-granular	Moldic (rect.)	Moldic (round)	Matrix Solution	Vuggy	Intra-Granular	Pore Origin**
8112.08	W	+		++			-	+	FS
8114.70	P	+		++		+	+	-	Dia.
8116.42	P	+		++		-	+		FS
8121.50	W	+		+		+	++		Dia.
8124.50	P	+		+			+	+	FS
8125.17	P	+		+	+			-	FS
8132.17	P	-		+	+	+	+		Dia.
8134.20	*P*	+							*Frac.*
8138.75	P	+		+	+	-			FS
8141.83	G	+	++	-			-	+	FS
8146.50	P	+	-	+		+		-	Dia.
8156.58	P	+	+	+		+		-	FS
8164.50	**G**		**++**	**-**					**Dep.**
8171.00	**W**	**++**		**-**	**-**			**-**	**Dep.**
8181.17	G		++	+		+		+	FS
8184.46	P	+		-		++		+	FS
8200.08	P	-				++			Dia.
8208.17	P	-	+				+	+	Dia.
8213.25	P	+			+	-	-	-	FS
8226.33	P	-	+	+	+	+	+	-	FS
8236.42	P	+		-		+			Dia.
8250.80	P	+		-		+	+	+	Dia.
8254.92	P	+					++		Dia.
8256.00	P	-				++			Dia.
8256.50	P	-				++		+	Dia.
8257.00	P/G		+		+		-	+	FS
8258.50	P/G		+	+			-	+	FS
8282.00	P	+	+	++		+		-	Dia.
8312.00	P		+	-	-			+	FS
8319.00	P/G	-	+	+	+		+	-	FS
8358.58	W	+		+	+				FS
8371.50	**P**	**+**	**-**	**+**					**Dep.**
8385.50	**W**	**+**		**-**	**-**				**Dep.**

Table 1**.** Continued.

Depth ***feet***	**Grain size***	**Matrix†**	**Inter-granular**	**Moldic (rect.)**	**Moldic (round)**	**Matrix Solution**	**Vuggy**	**Intra-granular**	**Pore Origin****
8396.50	**M**	**++**							**Dep.**
8447.70	**M**	**++**		**-**					**Dep.**
8454.25	**M**	**++**							**Dep.**
8461.80	W			+			++		Dia.
8462.67	P	-		+			+	+	Dia.
8476.00	**W**	**++**		**-**					**Dep.**
8488.50	W	-		+	+		+		Dia.
8499.40	**M**	**++**							**Dep.**
8522.50	**W**	**++**		**-**					**Dep.**
8538.00	W	+		+	+		-		FS
8551.20	W	++		+	-				FS
8555.20	P/G		++	+	+		-	+	FS
8604.25	P	+			+	+			FS
8604.92	W	+		-		+			FS
8608.67	P	+		-	++	+		-	Dia.
8614.67	W	+		+	+				FS
8620.50	W	+		+	+				FS
8622.40	W	-		+	+		-	-	Dia.
8623.67	W	++		+	+		+		FS
8625.25	W	+			++		+	+	Dia.
8628.17	W	+			+			+	FS
8635.10	P	-		-	+	+		-	FS
8639.20	P	-			-	++	-		Dia.
8645.70	P	-				++	-		Dia.
8651.33	P	+		-	+	+	+		FS
8657.50	P	+		-	+	+			FS
8659.80	W	+			+				FS
8663.70	W	+		-	-	+			FS
8664.50	W	+		+	+				FS
8727.00	**M**	**+**							**Dep.**
8745.50	**M**	**+**							**Dep.**
8760.70	**W**	**+**			**-**			**-**	**Dep.**

*M: Mudtsone; W: Wackestone; P: Packstone; G: Grainstone.

† Abundances: - present; + abundant; ++ very abundant.

** Dep.: Depositional; FS: Facies Selective; Dia.: Diagenetic; Frac.: Fracture

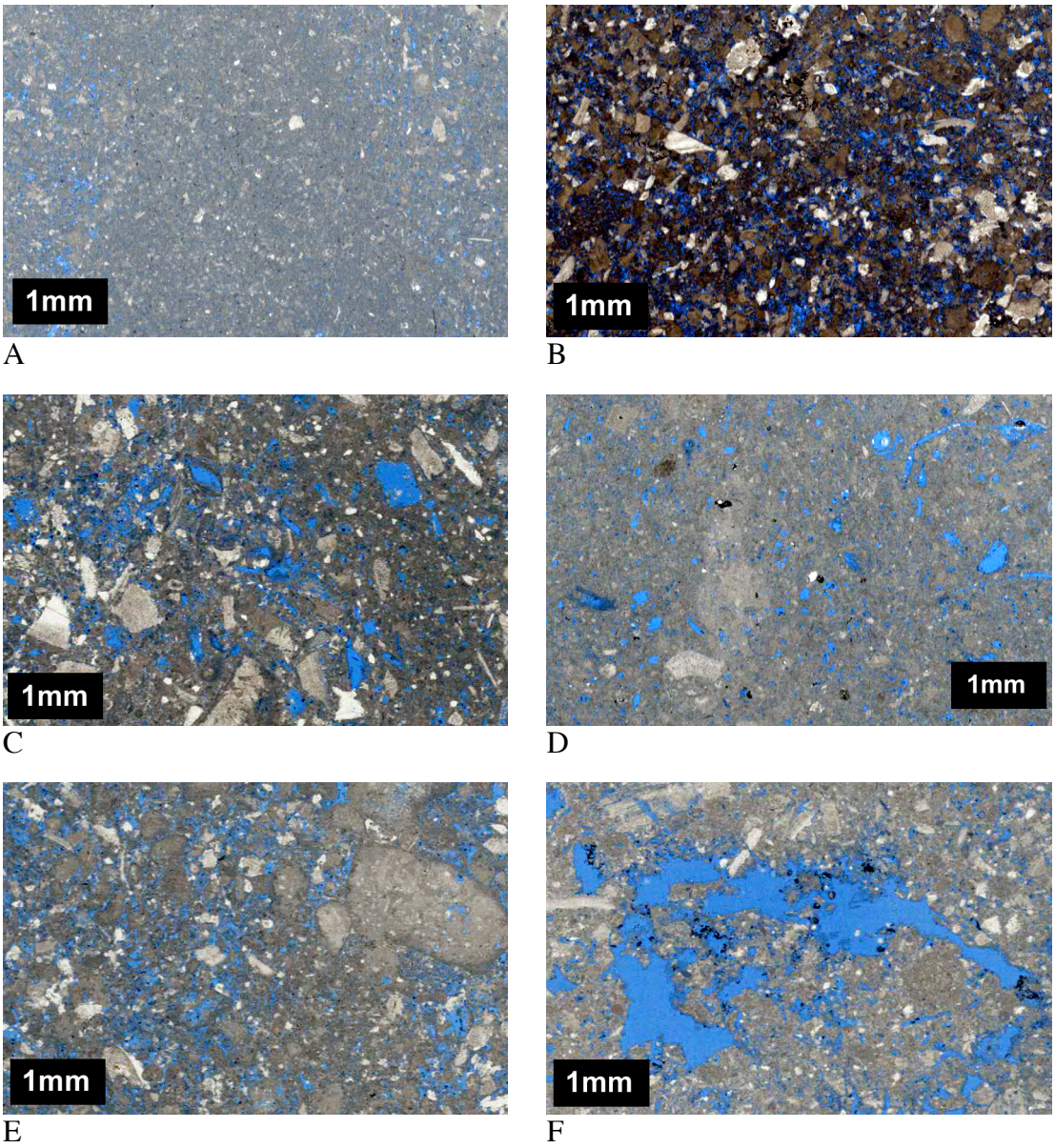

Figure 4. Photographs of observed pore types. A matrix/microporosity; B intergranular; C rectangular moldic; D roundish moldic; E matrix solution; F vuggy; G – I intragranular.

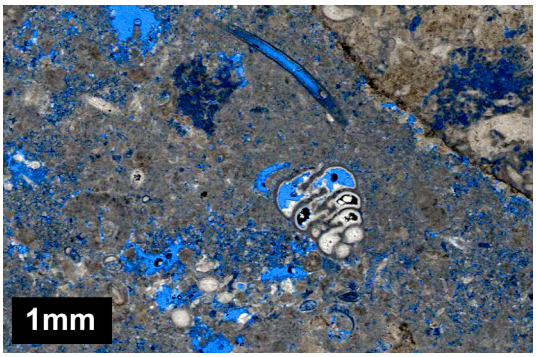

G

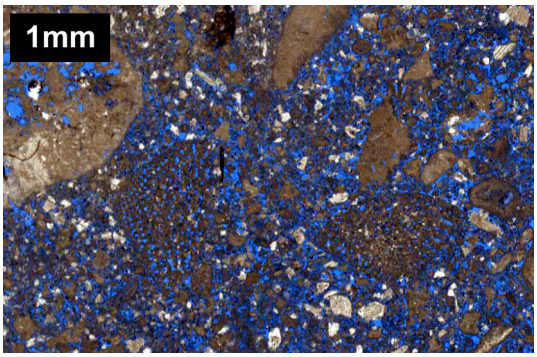

H

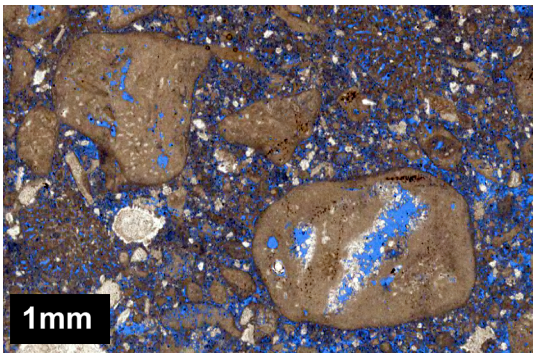

I

Figure 4. G – H intragranular.

Matrix solution porosity corresponds to the dissolution of some or all of the lime mud between grains in coarser-grained samples. It is therefore mostly observed towards the top of the core. Matrix solution porosity is however difficult to identify on thin-section photographs due to their limited resolution.

Vugs are present throughout the core and their presence usually indicates intensive diagenesis and usually a diagenetic origin for porosity of the sample.

Figure 5 shows the evolution of pore types along the core (depths are not to scale). The relative quantities reported are qualitative estimates, rather than quantitative proportions.

STATISTICAL ANALYSIS OF T2 DISTRIBUTIONS

Raw statistics of the NMR curve data are listed in Appendix A: arithmetic average, standard deviation (square root of sample variance), skewness, median, 90^{th} percentile and mode. Also shown is the average value of each parameter. Figure 6 shows cross-plots of these parameters versus genetic pore origin. We here define high discrimination power as no overlap of the range taken by a given parameter between each pore origin. Arithmetic average, mode, median and 90^{th} percentile all show good discrimination power. Standard deviation shows the smallest discrimination power. Skewness separates depositional porosity from other pore origins, but shows little separation between facies selective and diagenetic porosity. Variance-covariance and correlation matrices are shown in Table 2.

Principal components analysis

Running a principal component analysis on all of the estimated parameters isn't useful. First, the results would be too strongly influenced by skewness. Skewness has a very high variance when compared to the other parameters, yet has little discrimination power. Normalizing the data to arithmetic averages decreased this difference in variance.

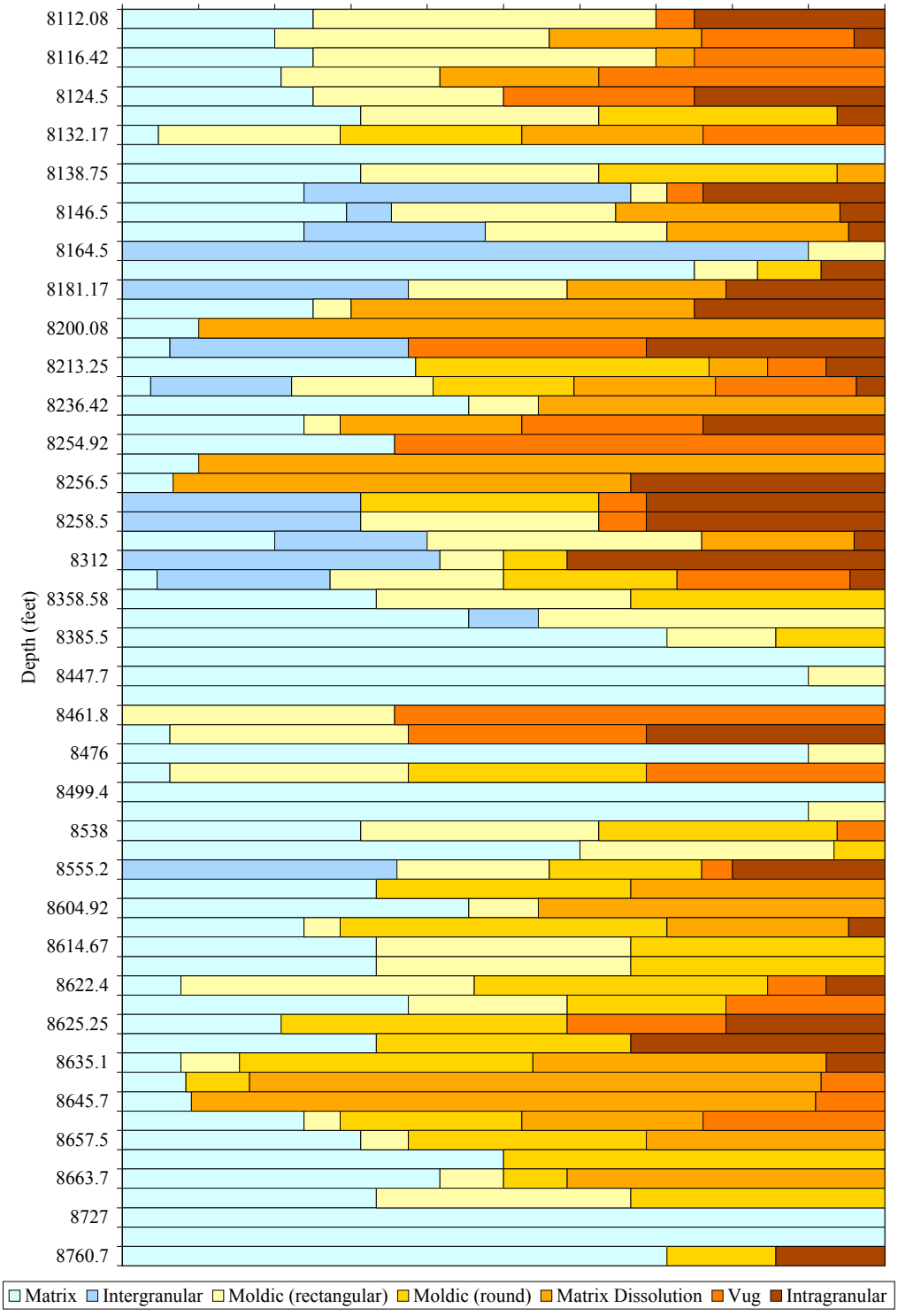

Figure 5. Qualitative evolution of porosity versus depth.

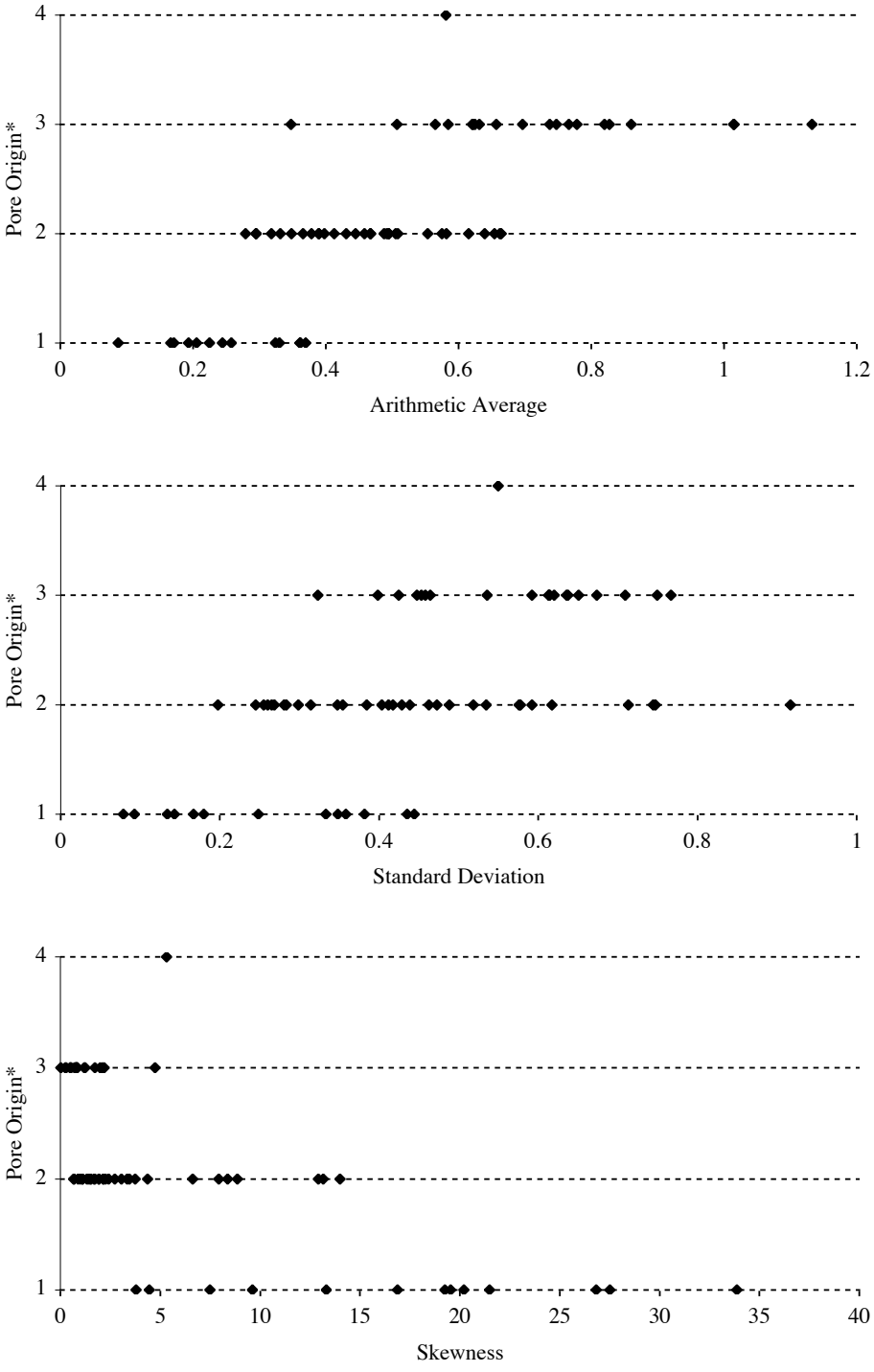

Figure 6. Cross-plots of genetic pore origin versus descriptive statistic parameters. Pore origin key: 1 Depositional; 2 Facies Selective; 3 Diagenetic; 4 Fracture.

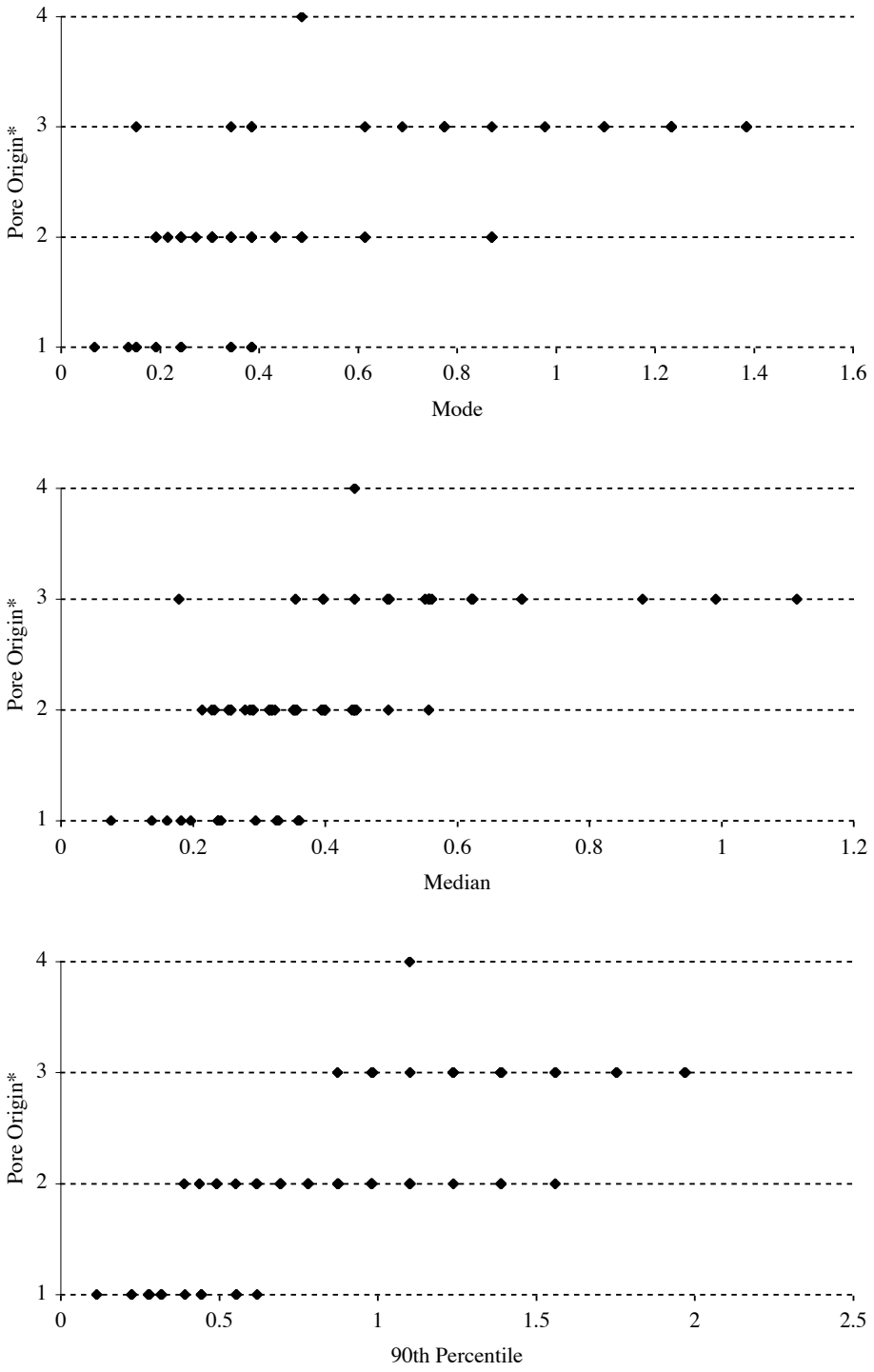

Figure 6. Continued.

Table 2. Variance-covariance and correlation matrices for statistical parameters.

		Arithmetic Average	Standard Deviation	Skewness	Mode	Median	90th Percentile
Variance-Covariance	Arithmetic Average	0.0471	0.0315	-0.8418	0.0696	0.0390	0.1012
	Standard Deviation		0.0344	-0.3784	0.0402	0.0221	0.0703
	Skewness			58.4789	-1.0694	-0.5478	-2.1480
	Mode				0.1284	0.0624	0.1447
	Median					0.0363	0.0772
	90th Percentile						0.2342
Correlation	Arithmetic Average	1.0000	0.7825	-0.5070	0.8953	0.9425	0.9630
	Standard Deviation		1.0000	-0.2667	0.6050	0.6238	0.7829
	Skewness			1.0000	-0.3903	-0.3759	-0.5804
	Mode				1.0000	0.9138	0.8344
	Median					1.0000	0.8374
	90th Percentile						1.0000

However, variance of skewness remained an order of magnitude higher than for the other parameters. Second, standard deviation also has little discrimination power and is best left out. Third, Table 2 shows that several parameters are strongly correlated (e.g. for arithmetic average and 90th percentile, $r = 0.96$).

Only mode and 90th percentile were retained for the principal component analysis. This is the result of eliminating skewness and standard deviation because of their low discrimination power, and by selecting the pair of parameters that exhibit the lowest coefficient of correlation. Median and arithmetic average were also eliminated as they showed strong correlation to respectively mode and 90th percentile. Including them in the analysis would introduce redundancy in the data.

The first and second principal components of the mode-90th percentile system respectively account for 92.5% and 7.5% of total variability. The resulting principal components are defined as:

$$PC1 = 1 \cdot \text{Mode} + 1.4306 \cdot 90^{th}\ \text{Percentile}$$

$$PC2 = 1 \cdot \text{Mode} - 0.6990 \cdot 90^{th}\ \text{Percentile}$$

Figure 7 shows a cross-plot of the mode-90th percentile data set transformed using these principal components. The single fracture porosity sample is not shown. The separation between different pore origins is not perfect, but usable for the conditional probabilities.

Conditional probabilities

The parameter retained for calculating the conditional probabilities is the first principal component of the mode-90th percentile system. The ideal range h for calculating these probabilities was estimated as 0.35 using:

$$h = \frac{5 \cdot \left(X_{\max} - X_{\min}\right)}{N} \quad \text{..... (23)}$$

Where N is the total number of samples. However, the estimated value of 0.35 was

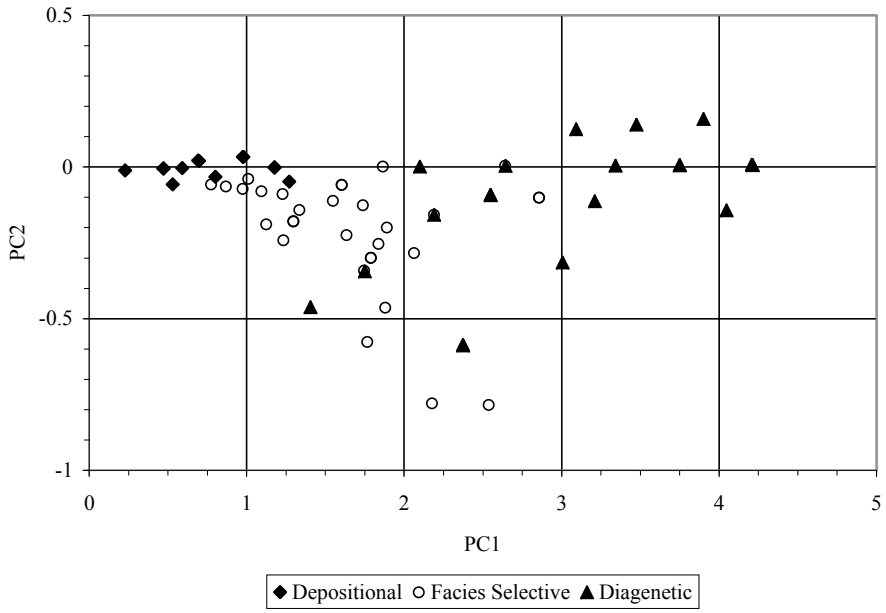

Figure 7. Principal component cross-plot for the mode-90th percentile system.

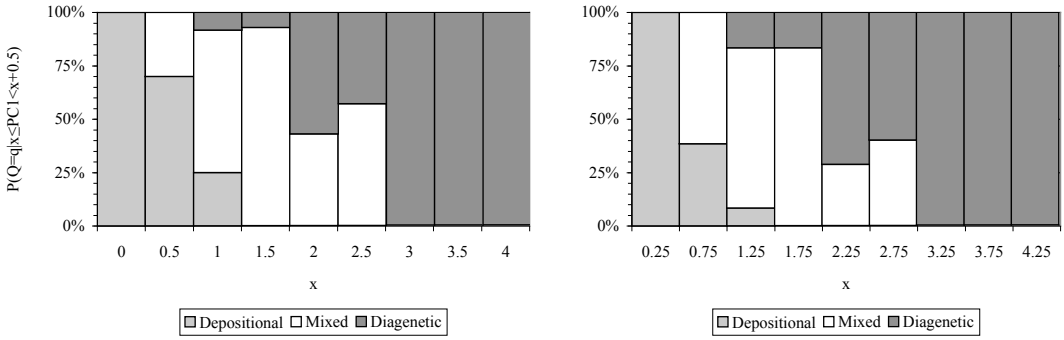

Figure 8. Conditional probability histograms for genetic pore origin.

too small and conditional probability values lacked consistency when the histogram bins were shifted. When the value of h was increased to 0.5, there was much greater consistency of the results. Conditional probabilities calculated with $h = 0.5$ and two different initialization points (0 and 0.25) are shown in figure 8.

Three zones may be identified on the conditional probability histogram. A lower zone (PC1 lower than 0.6/0.7) where depositional porosity has a probability of 100%; an intermediate zone where all three genetic pore origins coexist but where facies selective porosity predominates; and an upper zone (PC1 greater than 3) where diagenetic porosity has a probability of 100%. It should be noted that facies selective porosity never reaches a probability of 100%. It cannot therefore be predicted with as much confidence as the other two pore origins based on the data and statistics used in this study. Taking into account the second principal component or finding a more suitable statistic could however yield clearer results.

T2 MODELING USING LOG-NORMAL COMPONENTS

Three successive modeling runs named run 1, run 2 and run 3 were performed, respectively fitting 1, 2 and 3 log-normal distributions. The raw results are given in Appendices B through D. The average, standard deviation and weight for each individual distribution, as well as multiplying factor and SSE of the complete model are shown. The coefficients of determination for all three runs are given in appendix E. These parameters correspond to the parameters used for the log-transformed space and not the raw values.

A cross-plot of the multiplying coefficient versus NMR porosity for run 3 is shown in Figure 9. There is a very strong relationship between the two parameters, with the exception of one point. This point corresponds to a depositional porosity sample with a poor fit. The relatively low multiplier coefficient compared to true porosity is due to the high standard deviation of one of the distribution's log-normal components.

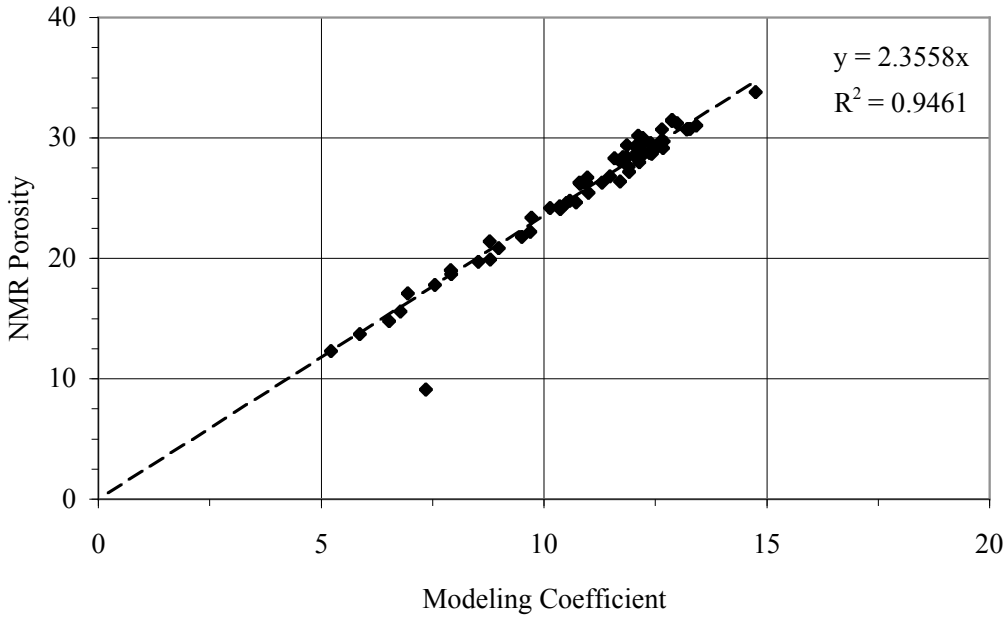

Figure 9. Modeling coefficient *A* versus NMR porosity cross-plot (run 3).

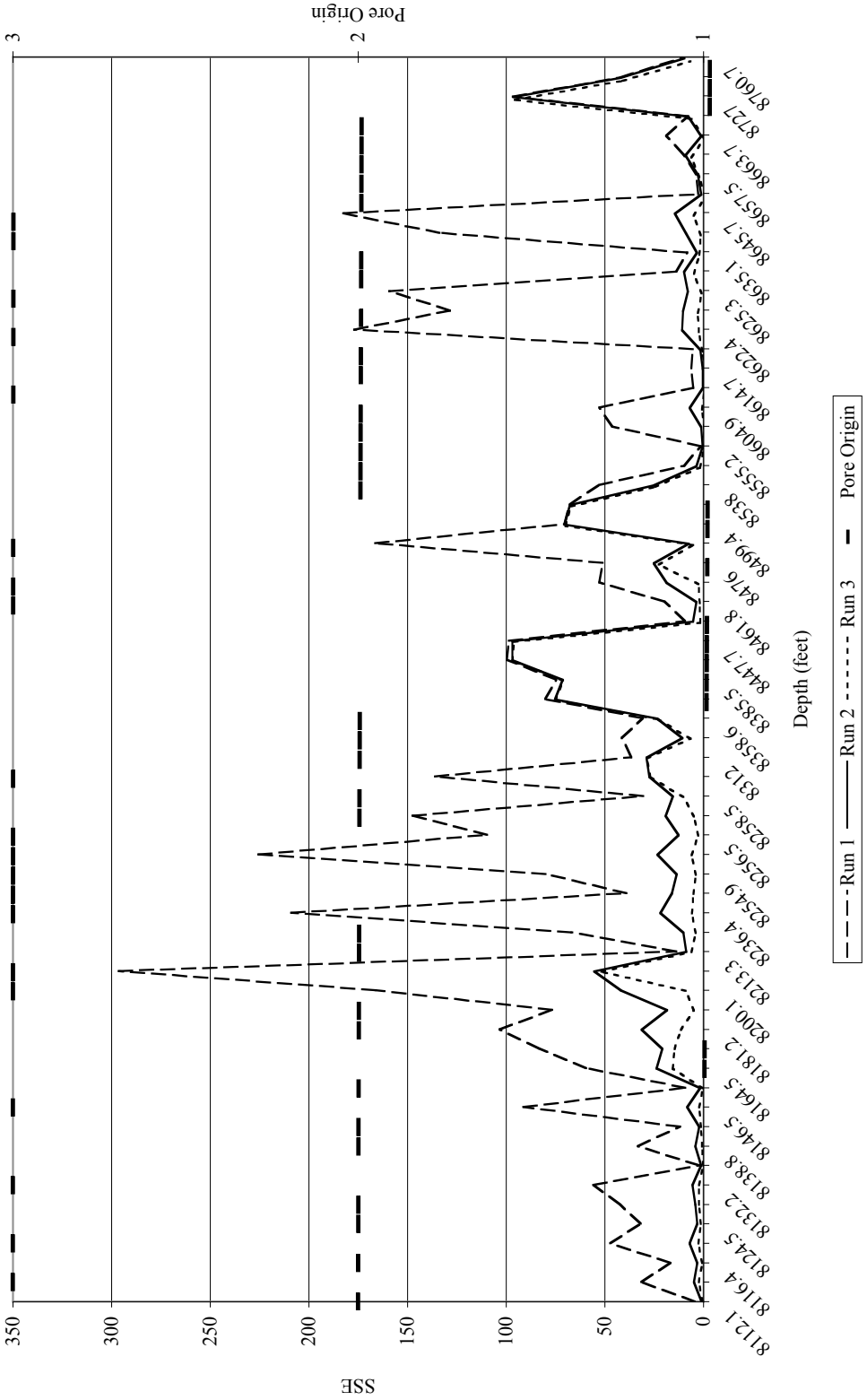

Figure 10. SSE values versus depth. Pore origin key: 1 Depositional; 2 Facies Selective; 3 Diagenetic.

The sum of squared error (SSE) versus depth for the 3 modeling runs is shown in Figure 10. The genetic pore origin of the samples is also shown. The SSE is much more variable for the first run than it is in the following two runs. This demonstrates the heterogeneity of fit quality when only one distribution is used. Along with being less variable, SSE values for runs 2 & 3 are also relatively low. This indicates that good fits are obtained when two or more distributions are considered. Depositional porosity seldom shows low SSE values, no matter how many distributions are fitted.

The evolution of R^2 versus depth is shown in Figure 11. Again, genetic origin of porosity is overlain on this plot. As shown in Figure 10, high variation of R^2 for run 1; lower variability and higher values for runs 2 and 3. However, if depositional porosity samples still have generally lower R^2 values than the other samples, its R^2 values remain high (around 0.98), showing a strong correlation between modeled and measured data.

In order to better interpret the improvement provided by increasing numbers of fitted distributions, normalized R^2 increase was calculated. These increases are shown versus depth and pore origin in Figure 12 and were calculated as follows:

$$\Delta R^2 = \frac{\left(R_i^2 - R_{i+n}^2\right)}{R_i^2} \quad \text{..... (24)}$$

where i is the run number. As expected from Figure 11, the general improvement between runs 1 and 2 is high and accounts for most of the total improvement. Improvement is generally low for depositional porosity, with improvement increasing with facies selective and diagenetic porosity. Figure 13 is identical to Figure 12, but data have been sorted by genetic pore origin. This figure clearly shows the variations in R^2 improvement between the different pore origins. Depositional porosity generally indicates no improvement, whereas facies selective and diagenetic show increasing improvements. Hence, depositional porosity appears to be adequately fitted by a single distribution. The discrepancies between depositional porosity and facies selective/diagenetic porosity in final fit quality (as defined by R^2 of run 3), will be discussed later on.

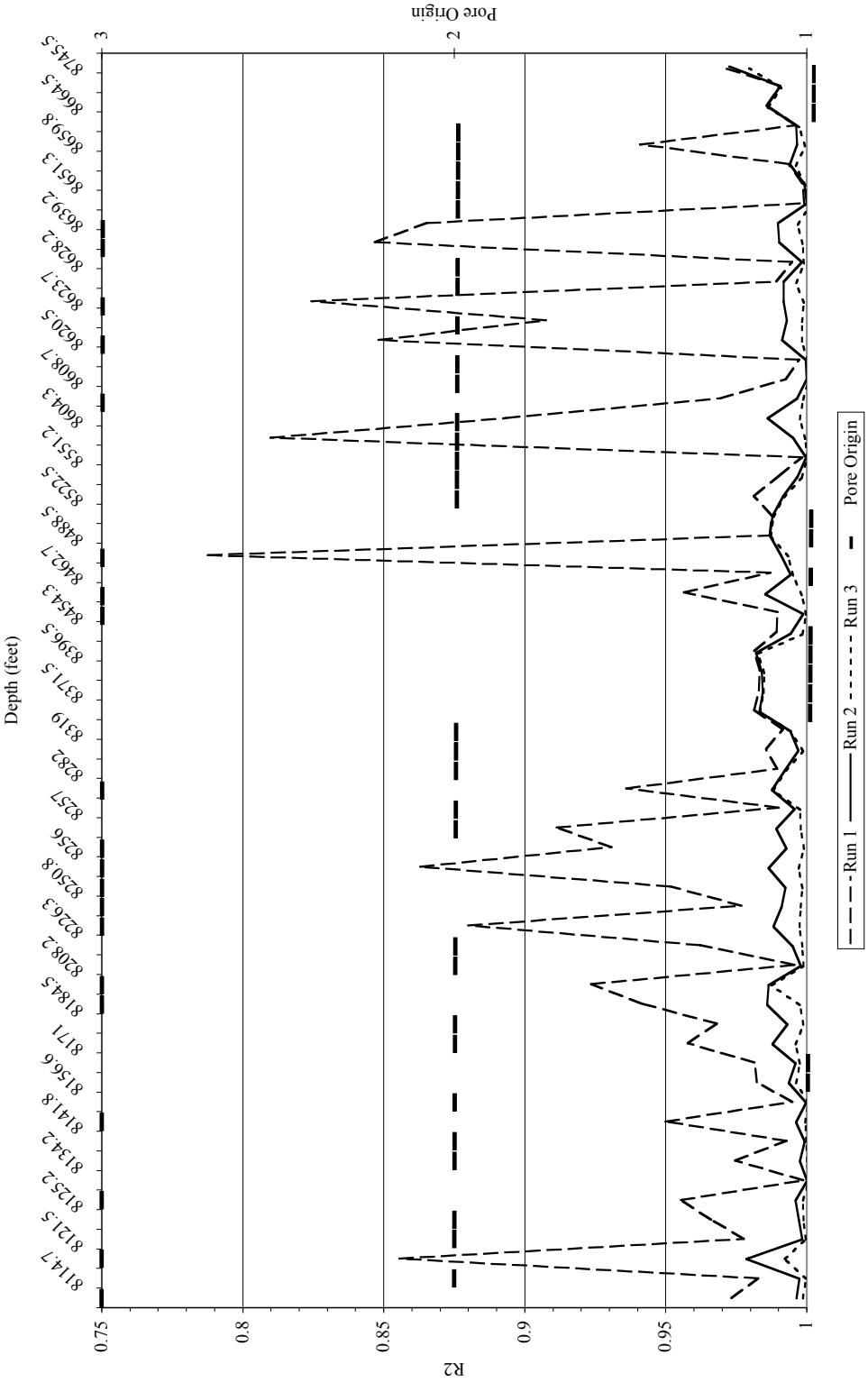

Figure 11. R^2 values versus depth. Pore origin key: 1 Depositional; 2 Facies Selective; 3 Diagenetic.

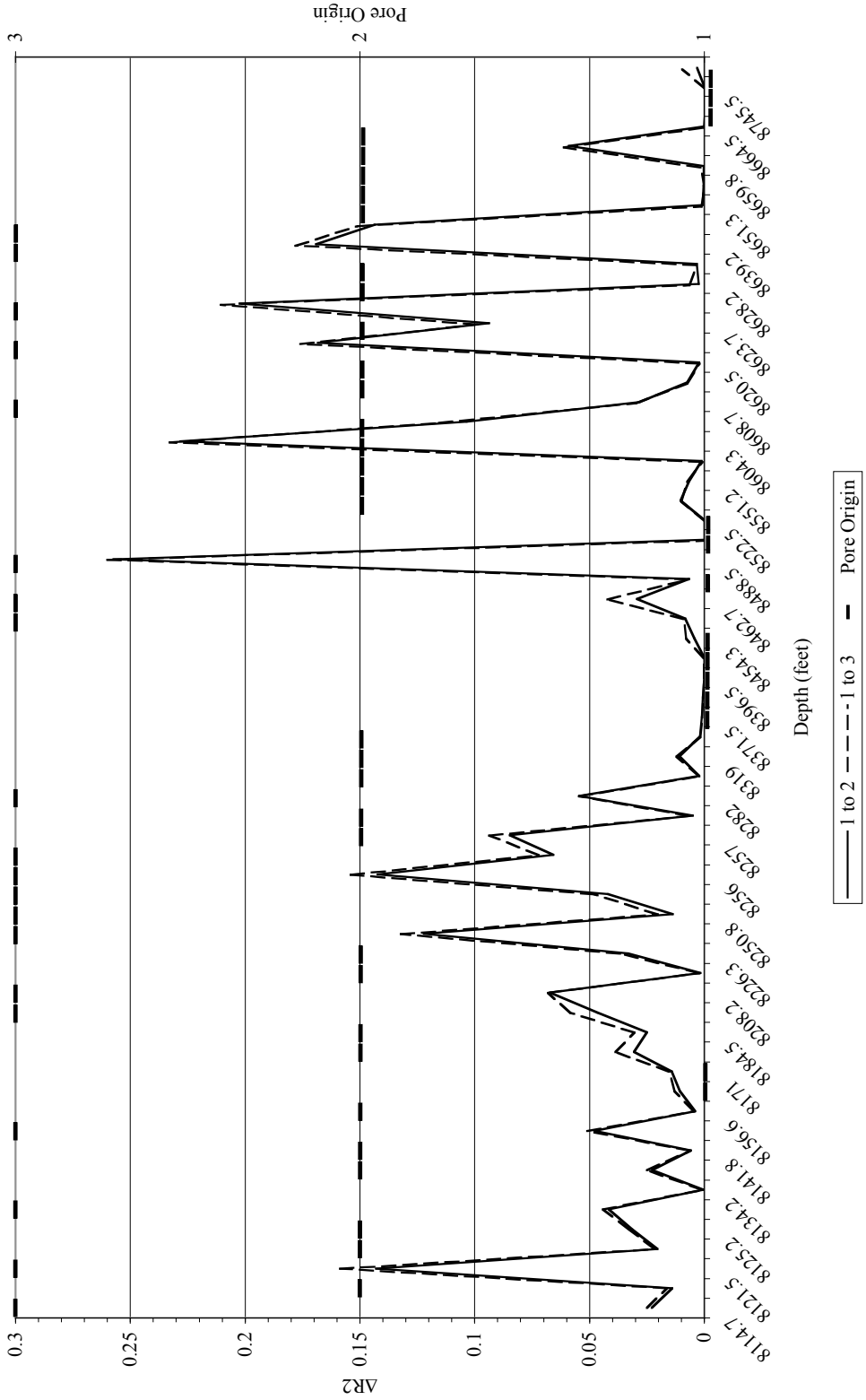

Figure 12. Normalized R^2 increase versus depth. Pore origin key: 1 Depositional; 2 Facies Selective; 3 Diagenetic.

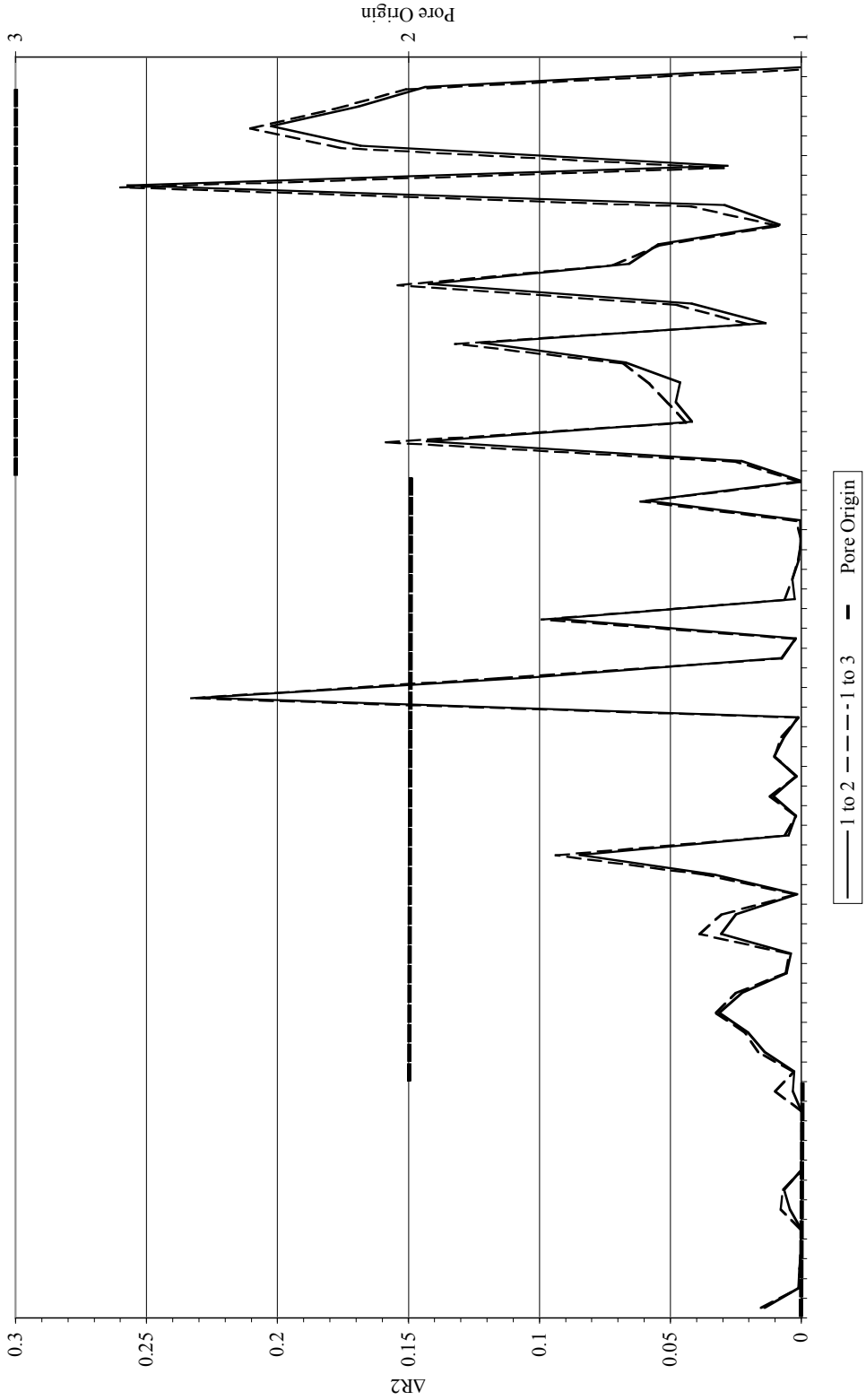

Figure 13. Normalized R^2 increase versus pore origin. Pore origin key: 1 Depositional; 2 Facies Selective; 3 Diagenetic.

To better quantify this difference between depositional, facies selective and diagenetic porosity, arithmetic average and standard deviation of R^2 for all runs were calculated for each pore origin. Results are shown in Figure 14. Depositional porosity has a different behavior than porosities of the other two origins. Depositional porosity is characterized by both a constant average and a constant standard deviation. This implies that no improvement is achieved by using multiple distribution. In contrast, facies selective and diagenetic porosities show a strong increase in R^2 average and a strong decrease in standard deviation. Variations are greatest for diagenetic porosity. Two distributions yield generally good fits, indicated by a high average and low standard deviation. The third distributions only provides minor improvements.

This difference in behavior between pore origins can be used to identify pore types. Conditional probabilities were calculated on the normalized increase of R^2. The distribution of this increase is highly asymmetrical, with most data being between 0 and 0.05 and a maximum of 0.25. The use of a constant value for h would not yield representative conditional probabilities throughout. Conditional probabilities were therefore calculated for three asymmetrical intervals (Table 3).

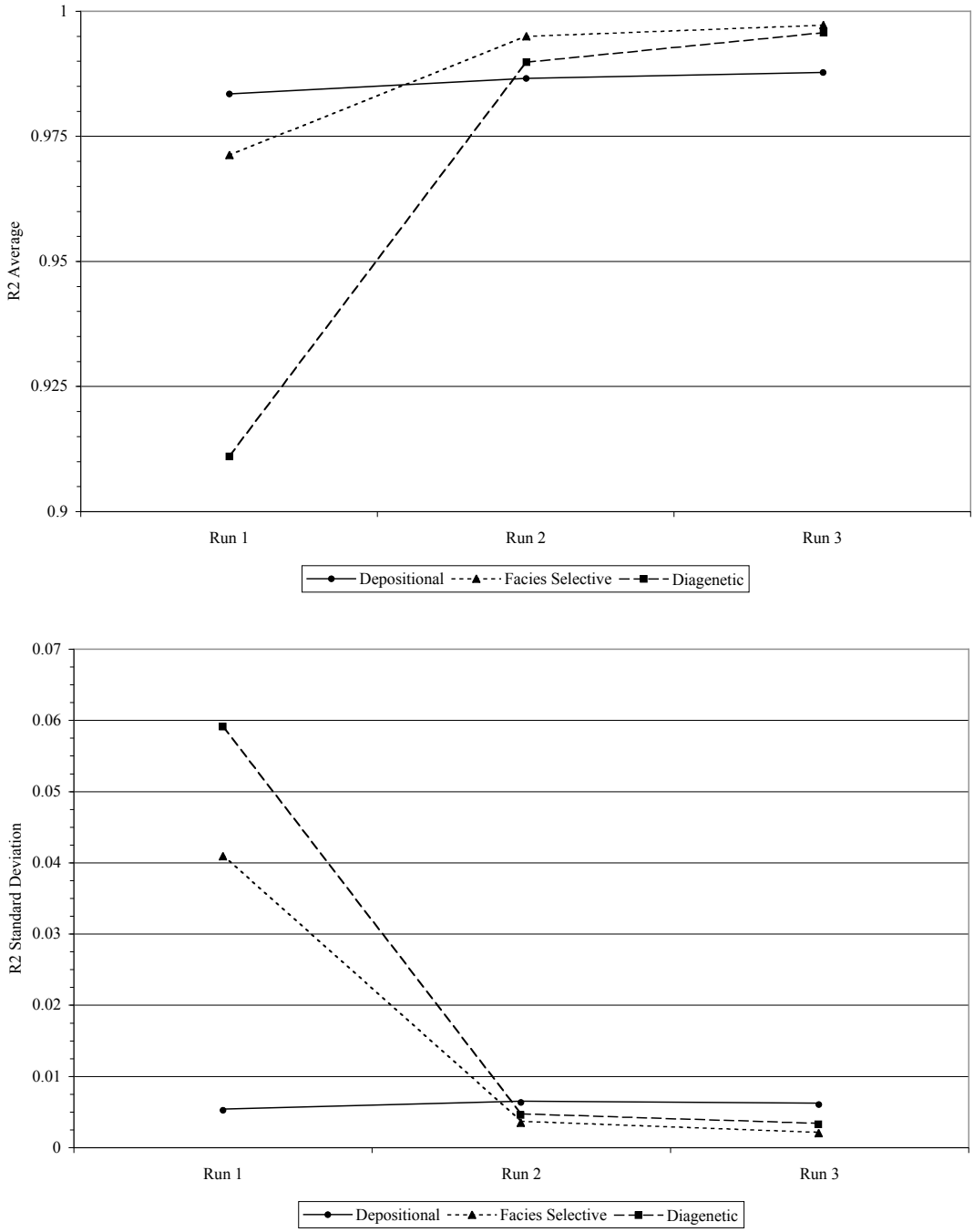

Figure 14. Average and standard deviation of R^2 for each genetic pore origin.

Table 3. Conditional probabilities for R^2.

$[x, x+h[\rightarrow$	**0-0.0004**	**0.0004-0.04**	**0.04-1**
$P(\text{Origin} = \text{Dep} \mid x \leq \Delta R^2 < x + h)$	100%	17.6%	0%
$P(\text{Origin} = \text{FS} \mid x \leq \Delta R^2 < x + h)$	0%	62.9%	17.7%
$P(\text{Origin} = \text{Diag} \mid x \leq \Delta R^2 < x + h)$	0%	19.5%	82.3%

DISCUSSION

SHAPE OF NMR CURVES

This study interprets T_2 distribution curve shape in terms of pore types and genetic origin. The T_2 distribution reflects a combined distribution of surface to volume ratios and surface relaxivities of all pores. To interpret the shape of the T_2 distribution curve, we must thus assume that surface relaxivity is constant throughout the sample, that the surface to volume ratio remains constant within a given pore type and that the size of each individual pore type follows a known uni-modal distribution.

Quintero *et al.* (1999) note that mud-supported samples have lower surface relaxivities than grain-supported samples, and hence both mudstones and grainstones may have the same T_2 times. They also note that mudstones have narrow T_2 distributions whereas grainstones will have broader ones. Standard deviation did not show to be a good pore type/origin characterizer in this study. This is most likely due to the fact that many distributions are multi-modal, resulting in a high variability in the measured standard deviation.

Variability of surface to volume ratio within a given pore type is difficult to assess. Indeed it may be invariant (e.g. intergranular porosity with spherical grains) or highly variable (e.g. porosity in dissolved rudistid fragments of varying shape). Surface to volume ratio may also be invariant for rudistid fragments if the shape of the fragments remains constant.

There is a fundamental problem of non-uniqueness: various combinations of surface to volume ratio, pore size and surface relaxivity may yield the same T_2 values and distributions. This will cause problems in trying to invert T_2 values into pore type and size. However, knowing possible pore shapes present in rock may help limit the solutions.

ACCURACY OF THE CONDITIONAL PROBABILITIES

The accuracy of the conditional probabilities is directly linked to the accuracy of the identification of pore characteristics from the thin section photographs. If the pore origin determined from the thin section photographs is incorrect, then the resulting conditional probabilities will be unsuitable.

Conditional probabilities predict pore origin from the first principal component relatively accurately. This is most likely due to the nature of depositional porosity and subsequent diagenetic porosity. As depositional porosity is matrix microporosity and diagenesis tends to increase pore size, they are easy to distinguish by low and high values for mode and 90^{th} percentile respectively.

The relatively large "transition" zone between facies selective and diagenetic porosity reflects the diffuse limit between the two pore origins in the genetic classification. This may also be the result of the variability of pore types present in each sample and what the signature of each pore type in the principal component is.

Finally, the accuracy of the conditional probabilities is influenced by the choice of statistics that are used in the principal component analysis. Though the selected parameters yielded good results, a different combination of statistics may show better results.

T2 MODELING RESULTS

The T_2 modeling is based on two main hypotheses: 1) that the T_2 distribution is the sum of multiple distribution representing different pore types discussed above and 2) that the NMR curves follow log-normal or multiple log-normal distributions. Log-normality was initially suspected due to the characteristic shape of the T_2 distributions. This was confirmed by probability plots in the case of simple depositional porosity. However probability plots are difficult to interpret in more complex T_2 distributions due

to the possible coexistence of multiple distributions and distribution types, as well as truncated distributions. Low SSE and large R^2 values give confidence in the choice of log-normal distributions.

The generally good fits obtained with multiple log-normal distributions tend to confirm that various unimodal T_2 distributions coexist. The problem however lays in interpreting the significance of these independent distributions in terms of pore type and size. It is difficult to determine whether the distributions correspond to different pore type, or different size/surface to volume ratios within an individual pore type.

The SSE for depositional porosity samples mostly show bad fits with values reaching 100 (to be compared with values lower than 1 for both facies selective and diagenetic porosity), regardless of how many distributions are used. The coefficient of determination R^2 shows better results, but depositional porosity still isn't fitted as well as facies selective and diagenetic porosity. This may be due to the fact that depositional (*i.e.* matrix) porosity does not follow a log-normal distribution. Figure 15 shows the modeled distribution for a sample with depositional porosity. The absolute error of the model is relatively constant throughout the distribution, indicating a distribution that is non-log-normal. If this is true, then identifying the distribution type(s) that best fits the NMR data for depositional porosity is potentially another tool for identifying pore types. The discrepancies could however be credited to the discrete nature of the T_2 distribution. For such a narrow distribution, only few data points are available for calculating the best fit. The divergence of one of the data points from a theoretically log-normal distribution will then make modeling more difficult and will greatly reduce the quality of the fit.

Conditional probabilities however are not the ideal tool for interpreting the results of this modeling. The modeling yields many parameters (averages, standard deviation, proportions and fit quality), all of which may contain important information. A neural network could be better suited at analyzing these results as it would allow a more synthetic approach. A neural network would however be constrained by the same

hypotheses and limits as conditional probabilities. Once trained, such a network could be used as a predicting tool for pore type based on modeling parameters.

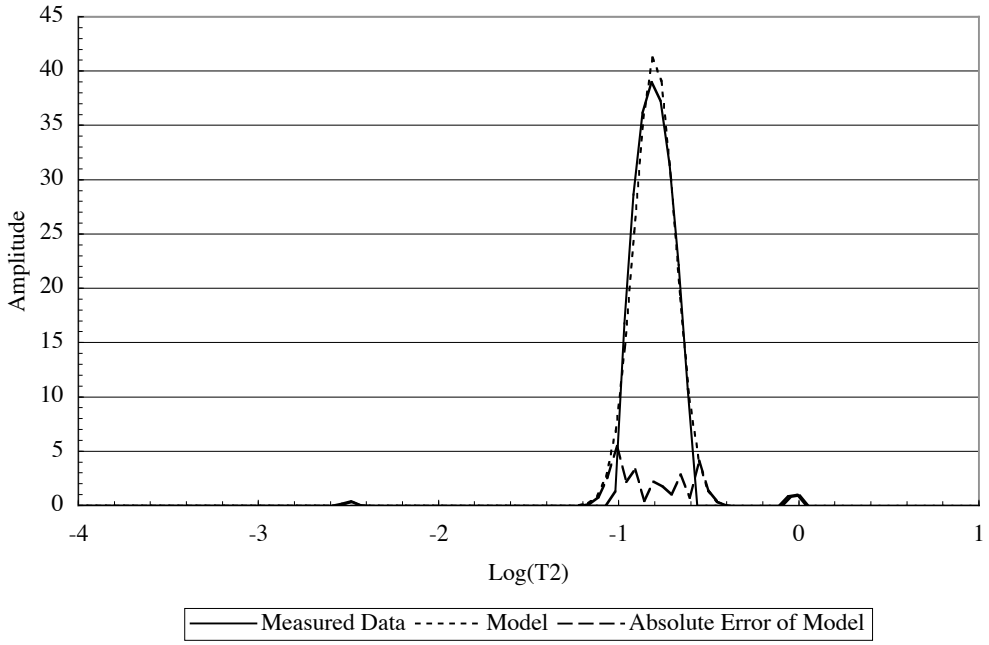

Figure 15. Example of fit quality for depositional porosity (depth of sample: 8727').

CONCLUSIONS

The objective of this study was to find relationships between pore characteristics and NMR data. This was successfully achieved by comparing thin section photograph interpretations to statistical analysis and modeling of NMR data. The comparisons were done by using conditional probabilities. Conditional probabilities were calculated for the first principal component of the mode-90^{th} percentile system as well as for the coefficient of determination R^2 of the NMR curve modeling.

The results were quite encouraging for the statistical analysis with a good predictability of pore origin using the first principal component. It is thought that this is linked to the fact that depositional porosity is mainly matrix/microporosity and is thus easy to differentiate from larger diagenetic porosity. Results for the modeling were however mixed. The quality of the fits between model and measured data was good and different pore origins behaved differently according to the number of fitted distributions. Depositional porosity should no improvement in fit quality however many distributions were used, whereas facies selective and diagenetic porosities showed increasing fit quality with increasing number of distributions. Despite this, the methods used in this study were not able to fully exploit the results of the modeling. Neural networks could be more useful and would allow comparison of the complete modeling data set (including averages, standard deviations and proportions) to the pore type data. Once trained, the neural network could be used to predict pore types based on the modeling results.

Besides using neural networks, work beyond this study should look into forward modeling of NMR data. This has the advantage of having control over the pore characteristics and can be done in two ways. First, artificial rock samples can be created and have routine NMR experimentation run on them. Second, statistics can be used to generate porous systems with control on shape, size and number of pores. This porous system can then be converted into a T_2 distribution.

REFERENCES CITED

Ahr, W. M., 1999, GEOL-624 Carbonate Reservoirs, Course Notes, Texas A&M University.

al-Awar, A. A., J. D. Humphrey, 2000, Diageneis of the Aptian Shuaiba formation at Ghaba North field, Oman: SEPM Special Publication, v. 69, p. 173-184.

Alsharhan, A. S., H. al-Aasm, M. G. Salah, 2000, Stratigraphy, stable isotopes, and hydrocarbon potential of the Aptian Shuaiba formation, U.A.E.: SEPM Special Publication, v. 69, p. 299-314.

Ausbrooks, R., N. F. Hurley, A. May, D. G. Neese, 1999, Pore-size distribution in vuggy carbonates from core images, NMR, and capillary pressure: SPE Technical Paper 56506, 1999 SPE Annual Technical Conference and Exhibition, Houston.

Chang, C., H. Vinegar, C. Morriss, C. Straley, 1994, Effective porosity, producible fluid, and permeability in carbonates from NMR logging: The Log Analyst, v. 38, no. 2, p. 60-72.

Choquette, P. W., L. C. Pray, 1970, Geologic nomenclature and classification of porosity in sedimentary carbonates: AAPG Bulletin, v. 54, no. 2, p. 207-244.

Coates, G. R., L. Xiao, M. G. Prammer, 1999, NMR Logging principles and applications: Houston, Halliburton Energy Services, 233 p.

Davis, J. C., 1986, Statistics and data analysis in geology: New York, John Wiley & Sons, 646 p.

Fisz, M., 1980, Probability theory and mathematical statistics: Malabar (Florida), Robert E. Krieger Publishing Company, 667 p.

Logan, W. D., J. P. Horkowitz, R. Laronga, D. W. Cromwell, 1998, Practical application of NMR logging in carbonate reservoirs: SPE Reservoir Evaluation & Engineering, October, p. 438-448.

Lyne, A., G. Varini, G. Ghilardotti, 1996, Determination of petrophysical properties of carbonate rocks by NMR relaxometry: SPE Technical Paper 36852, 1996 SPE European Petroleum Conference, Milan.

Quintero, L., A. Boyd, F. al-Wazeer, 1999, Comparison of permeability from NMR and production analysis in carbonate reservoirs: SPE Technical Paper 56798, 1999 SPE Annual Technical Conference and Exhibition, Houston.

Russell, S. D., M. Akbar, B. Vissapragada, G. M. Walkden, 2002, Rock types and permeability prediction from dipmeter and image logs: Shuaiba reservoir (Aptian), Abu Dhabi): AAPG Bulletin, v. 86, no. 10, p. 1709-1732.

APPENDIX A

Descriptive statistics analysis of NMR curve results.

Depth *feet*	Arithmetic Average *sec*	Standard Deviation *sec*	Skewness	Mode *sec*	Median *sec*	90th Percentile *sec*
8112.08	0.4451	0.4175	1.9240	0.3430	0.3152	0.9799
8114.7	0.7373	0.5920	1.1880	0.7743	0.5568	1.5593
8116.42	0.4951	0.4035	1.3398	0.4329	0.3958	0.9809
8121.5	0.8606	0.7496	0.8235	1.2329	0.6969	1.9672
8124.5	0.5089	0.4624	1.6818	0.3054	0.3536	1.1005
8125.17	0.6545	0.6170	1.4092	0.3054	0.3941	1.5591
8132.17	0.6968	0.6132	1.2373	0.9770	0.4940	1.5595
8134.2	0.5813	0.5496	5.3172	0.4863	0.4443	1.1010
8138.75	0.5751	0.4285	1.1026	0.6136	0.4437	1.1020
8141.83	0.6395	0.9169	6.6153	0.4863	0.4436	1.1011
8146.5	0.5653	0.4478	4.7299	0.6136	0.4445	1.1020
8156.58	0.4680	0.3847	2.2550	0.3854	0.3566	0.8730
8164.5	0.3696	0.3817	19.2478	0.3854	0.3592	0.6195
8171	0.3618	0.4354	19.5361	0.3854	0.3261	0.5531
8181.17	0.4587	0.5777	13.1457	0.4863	0.3992	0.7800
8184.46	0.4668	0.4885	14.0065	0.4863	0.3995	0.7803
8200.08	0.5845	0.3230	0.2902	0.6893	0.5609	0.9842
8208.17	1.1326	0.6736	0.0150	1.3849	1.1137	1.9702
8213.25	0.3654	0.2836	3.7338	0.3054	0.2900	0.5515
8226.33	0.6646	0.5184	1.0017	0.8697	0.4957	1.3892
8236.42	0.6208	0.4247	0.5256	0.8697	0.5574	1.2380
8250.8	0.6250	0.6131	2.0992	0.3854	0.3975	1.3873
8254.92	0.6222	0.4534	0.8486	0.7743	0.4967	1.2376
8256	0.7474	0.5359	0.5086	1.0975	0.6238	1.3912
8256.5	0.6571	0.4644	0.7654	0.7743	0.5570	1.2381
8257	0.6626	0.4727	0.6679	0.8697	0.5568	1.2385
8258.5	0.4921	0.7130	8.8556	0.4329	0.3999	0.7787
8282	1.0146	0.6374	0.2446	1.2329	0.9909	1.7546
8312	0.3894	0.5347	12.9134	0.3430	0.3237	0.6188
8319	0.4950	0.2808	0.6853	0.4863	0.4471	0.8751
8358.58	0.3178	0.1974	3.0459	0.3054	0.2912	0.4921
8371.5	0.3608	0.2484	21.4817	0.3854	0.3610	0.5543
8385.5	0.3299	0.4442	20.1951	0.3430	0.2944	0.4427

Depth *feet*	Arithmetic Average *sec*	Standard Deviation *sec*	Skewness	Mode *sec*	Median *sec*	90th Percentile *sec*
8396.5	0.3238	0.1796	33.8739	0.3430	0.3288	0.4439
8447.7	0.2441	0.3331	27.5033	0.2420	0.2419	0.3182
8454.25	0.2056	0.3584	13.3197	0.1353	0.1373	0.2758
8461.8	0.5072	0.4579	2.1977	0.3430	0.3552	0.9798
8462.67	0.6314	0.6507	2.0019	0.3854	0.3966	1.3874
8476	0.2579	0.1671	3.7850	0.2420	0.2375	0.3919
8488.5	0.8203	0.7090	0.7966	1.3849	0.5512	1.7528
8499.4	0.2249	0.1426	16.8674	0.2420	0.2380	0.3153
8522.5	0.1931	0.0929	9.6114	0.1918	0.1961	0.2799
8538	0.2789	0.2602	3.4644	0.2154	0.2134	0.3894
8551.2	0.3481	0.3144	2.1434	0.2420	0.2535	0.6921
8555.2	0.4882	0.4119	1.7272	0.3854	0.3542	0.9803
8604.25	0.6153	0.5759	1.1095	0.8697	0.4401	1.3887
8604.92	0.4309	0.3546	0.8900	0.6136	0.3514	0.8747
8608.67	0.3478	0.3982	1.7267	0.1520	0.1783	0.8726
8614.67	0.5051	0.7475	7.9393	0.3854	0.3156	0.9801
8620.5	0.3316	0.2550	2.1450	0.2420	0.2565	0.6165
8622.4	0.7784	0.6143	0.7705	1.2329	0.6215	1.5610
8623.67	0.4129	0.4388	1.9255	0.1918	0.2282	1.1002
8625.25	0.8274	0.6356	0.6990	1.2329	0.6981	1.7523
8628.17	0.2953	0.2651	3.3419	0.2420	0.2325	0.4373
8635.1	0.5818	0.7444	8.3705	0.4863	0.4447	0.9813
8639.2	1.0153	0.7669	0.4821	1.3849	0.8805	1.9688
8645.7	0.7668	0.6197	0.8495	1.0975	0.6218	1.5606
8651.33	0.3982	0.3477	2.7189	0.3054	0.2861	0.6925
8657.5	0.3901	0.2984	2.4067	0.3430	0.3191	0.6933
8659.8	0.2946	0.2451	4.3645	0.2719	0.2572	0.4909
8663.7	0.5538	0.5919	1.5248	0.1918	0.2789	1.3881
8664.5	0.3786	0.2686	1.5038	0.3054	0.3192	0.6930
8727	0.1667	0.0787	7.4785	0.1520	0.1817	0.2237
8745.5	0.1712	0.3484	26.8115	0.1520	0.1608	0.2238
8760.7	0.0872	0.1340	4.4503	0.0673	0.0755	0.1130
Average	0.5052	0.4476	5.7267	0.5311	0.4036	0.9643

APPENDIX B

Results of T_2 modeling, run 1.

Depth *feet*	Average $log(T_2)$	Standard Deviation $log(T_2)$	Multiplier	SSE
8112.08	-0.481	0.411	10.83	4.29
8114.70	-0.179	0.364	10.21	31.57
8116.42	-0.371	0.363	9.24	16.67
8121.50	-0.019	0.365	5.41	47.41
8124.50	-0.455	0.379	11.34	31.79
8125.17	-0.342	0.468	12.18	42.17
8132.17	-0.292	0.479	12.24	55.89
8134.20	-0.344	0.341	12.00	2.25
8138.75	-0.311	0.375	10.77	33.33
8141.83	-0.345	0.363	12.03	11.90
8146.50	-0.264	0.325	11.63	91.38
8156.58	-0.422	0.293	11.10	9.30
8164.50	-0.436	0.211	12.17	59.52
8171.00	-0.458	0.184	12.92	83.34
8181.17	-0.345	0.249	11.46	103.31
8184.46	-0.353	0.265	11.72	76.59
8200.08	-0.201	0.225	11.52	166.27
8208.17	0.142	0.169	11.52	296.43
8213.25	-0.512	0.229	12.22	13.73
8226.33	-0.251	0.403	13.07	66.94
8236.42	-0.166	0.287	10.31	209.03
8250.80	-0.349	0.343	11.80	38.98
8254.92	-0.244	0.363	11.80	80.00
8256.00	-0.060	0.275	9.85	225.62
8256.50	-0.198	0.342	11.05	109.79
8257.00	-0.171	0.328	11.04	147.62
8258.50	-0.388	0.240	12.60	30.57
8282.00	0.075	0.210	9.74	136.08
8312.00	-0.454	0.211	12.33	36.58
8319.00	-0.330	0.264	12.82	41.62
8358.58	-0.530	0.191	11.92	30.74
8371.50	-0.438	0.193	12.98	80.33
8385.50	-0.514	0.176	12.36	74.68
8396.50	-0.492	0.151	13.26	99.69

Depth *feet*	Average $log(T_2)$	Standard Deviation $log(T_2)$	Multiplier	SSE
8447.70	-0.621	0.139	11.91	98.89
8454.25	-0.877	0.241	6.76	9.48
8461.80	-0.456	0.332	12.12	19.93
8462.67	-0.372	0.365	10.36	52.97
8476.00	-0.606	0.174	11.82	51.12
8488.50	-0.202	0.555	9.82	166.44
8499.40	-0.654	0.150	12.25	70.53
8522.50	-0.731	0.153	12.47	67.98
8538.00	-0.677	0.186	10.17	53.24
8551.20	-0.600	0.340	8.57	9.85
8555.20	-0.421	0.371	7.93	1.57
8604.25	-0.222	0.454	5.20	46.39
8604.92	-0.405	0.429	7.11	52.95
8608.67	-0.726	0.585	5.31	5.43
8614.67	-0.463	0.410	8.83	6.34
8620.50	-0.593	0.284	10.15	5.57
8622.40	-0.174	0.466	10.97	177.07
8623.67	-0.698	0.283	9.15	128.54
8625.25	-0.105	0.421	9.05	159.46
8628.17	-0.643	0.227	7.60	13.99
8635.10	-0.334	0.320	10.22	8.38
8639.20	0.114	0.223	6.42	134.01
8645.70	-0.173	0.455	11.86	182.86
8651.33	-0.528	0.298	10.68	2.94
8657.50	-0.480	0.284	10.90	3.95
8659.80	-0.588	0.244	8.65	10.25
8663.70	-0.492	0.577	7.06	19.14
8664.50	-0.485	0.273	10.42	8.09
8727.00	-0.807	0.113	11.72	96.82
8745.50	-0.831	0.157	11.31	42.36
8760.70	-1.195	0.209	3.94	11.14

APPENDIX C

Results of T_2 modeling, run 2.

Depth *feet*	Average 1 $log(T_2)$	Standard Deviation1 $log(T_2)$	Average 2 $log(T_2)$	Standard Deviation 2 $log(T_2)$	Ratio†	Multiplier	SSE
8112.08	-0.293	0.322	-0.660	0.397	0.43	10.83	1.26
8114.70	-0.073	0.277	-0.557	0.419	0.63	10.64	5.16
8116.42	-0.327	0.323	-1.031	0.492	0.81	9.80	3.35
8121.50	0.105	0.222	-0.555	0.558	0.49	6.30	7.27
8124.50	0.129	0.153	-0.510	0.311	0.13	11.27	3.33
8125.17	0.157	0.181	-0.481	0.357	0.22	11.84	4.40
8132.17	0.086	0.211	-0.521	0.374	0.32	11.95	5.93
8134.20	-0.075	0.244	-0.402	0.323	0.16	11.93	1.37
8138.75	-0.106	0.228	-0.528	0.359	0.40	10.83	4.34
8141.83	-0.179	0.267	-0.518	0.359	0.42	12.06	2.47
8146.50	-0.165	0.231	-0.674	0.390	0.60	12.46	8.38
8156.58	-0.421	0.291	-1.464	0.145	0.96	11.51	1.96
8164.50	-0.278	0.116	-0.513	0.188	0.27	12.03	24.10
8171.00	-0.323	0.098	-0.532	0.163	0.29	12.78	21.20
8181.17	-0.287	0.197	-0.702	0.337	0.67	12.40	31.67
8184.46	-0.243	0.180	-0.559	0.285	0.50	12.09	18.59
8200.08	-0.150	0.176	-0.585	0.340	0.65	12.95	42.00
8208.17	0.144	0.165	-0.671	0.228	0.78	14.49	55.47
8213.25	-0.387	0.171	-0.653	0.176	0.51	12.06	8.91
8226.33	0.051	0.180	-0.410	0.362	0.26	12.93	10.36
8236.42	-0.080	0.193	-0.683	0.385	0.58	12.00	22.07
8250.80	-0.241	0.399	-0.462	0.211	0.69	12.04	16.34
8254.92	-0.054	0.207	-0.487	0.365	0.41	12.05	13.90
8256.00	0.015	0.191	-0.629	0.431	0.57	12.02	23.52
8256.50	-0.065	0.215	-0.570	0.390	0.53	11.78	12.77
8257.00	-0.054	0.211	-0.596	0.414	0.54	12.16	19.37
8258.50	-0.387	0.239	-1.350	0.108	0.96	13.13	15.75
8282.00	0.096	0.188	-0.639	0.457	0.72	11.97	27.75
8312.00	-0.454	0.211	-1.482	0.095	0.97	12.69	29.06
8319.00	-0.145	0.151	-0.428	0.242	0.28	12.72	10.93
8358.58	-0.530	0.191	-1.576	0.084	0.97	12.24	23.78
8371.50	-0.438	0.193	-1.489	0.106	0.98	13.28	75.56

Depth *feet*	Average 1 $log(T_2)$	Standard Deviation1 $log(T_2)$	Average 2 $log(T_2)$	Standard Deviation 2 $log(T_2)$	Ratio†	Multiplier	SSE
8385.50	-0.514	0.176	-1.769	0.107	0.98	12.61	71.56
8396.50	-0.492	0.151	-1.555	0.061	0.99	13.43	97.09
8447.70	-0.621	0.138	-1.758	0.062	0.99	11.91	97.19
8454.25	0.126	0.123	-0.877	0.240	0.04	7.04	5.65
8461.80	-0.163	0.320	-0.564	0.260	0.36	12.25	3.99
8462.67	-0.264	0.462	-0.471	0.191	0.72	10.78	18.86
8476.00	-0.469	0.103	-0.677	0.144	0.31	11.63	25.49
8488.50	0.155	0.176	-0.607	0.375	0.43	9.50	7.73
8499.40	-0.154	0.513	-0.654	0.150	0.00	12.25	70.53
8522.50	-0.731	0.572	-0.731	0.153	0.00	12.47	67.98
8538.00	0.122	0.063	-0.677	0.186	0.05	10.73	25.43
8551.20	-0.450	0.319	-0.794	0.232	0.64	8.55	3.82
8555.20	-0.224	0.291	-0.535	0.357	0.32	7.92	0.66
8604.25	-0.072	0.264	-1.016	0.489	0.58	5.92	1.37
8604.92	-0.205	0.230	-0.813	0.483	0.45	7.58	7.22
8608.67	0.003	0.157	-0.815	0.501	0.11	5.21	0.73
8614.67	-0.240	0.281	-0.658	0.386	0.39	8.81	0.68
8620.50	0.078	0.095	-0.597	0.277	0.03	10.27	1.97
8622.40	0.077	0.196	-0.596	0.395	0.47	11.11	11.11
8623.67	0.081	0.162	-0.716	0.252	0.18	10.46	10.74
8625.25	0.080	0.199	-0.628	0.395	0.53	9.61	8.21
8628.17	-0.518	0.162	-0.794	0.166	0.53	7.48	10.31
8635.10	-0.128	0.219	-0.439	0.300	0.29	10.16	3.64
8639.20	0.124	0.209	-0.890	0.331	0.69	8.89	9.20
8645.70	0.051	0.215	-0.640	0.365	0.53	12.04	14.91
8651.33	-0.372	0.464	-0.540	0.279	0.17	10.87	1.38
8657.50	-0.295	0.188	-0.503	0.283	0.08	10.88	3.17
8659.80	-0.588	4.600	-0.588	0.242	0.12	9.71	9.57
8663.70	0.081	0.215	-0.709	0.407	0.27	6.82	1.34
8664.50	-0.485	0.572	-0.485	0.273	0.00	10.42	8.09
8727.00	-0.111	0.136	-0.807	0.113	0.00	11.74	96.60
8745.50	-0.831	0.178	-0.831	0.157	0.00	11.31	42.36
8760.70	-1.195	6.911	-1.195	0.205	0.35	5.89	9.99

†Represents proportion of distribution 1. Proportion of distribution 2 is 1 – *Ratio*.

APPENDIX D

Results of T_2 modeling, run 3.

Depth *feet*	Avg.1 $log(T_2)$	Std. Dev.1 $log(T_2)$	Avg.2 $log(T_2)$	Std. Dev.2 $log(T_2)$	Avg.3 $log(T_2)$	Std. Dev.3 $log(T_2)$	Weight 1	Weight 2	Weight 3	Multiplier	SSE
8112.08	-0.388	0.308	-0.737	0.391	-0.007	0.213	0.48	0.44	0.08	10.81	0.84
8114.70	-0.912	0.324	-0.277	0.277	0.071	0.212	0.15	0.55	0.31	10.59	2.59
8116.42	-1.225	0.403	-0.425	0.298	-0.058	0.203	0.13	0.69	0.17	9.72	0.94
8121.50	-1.090	0.678	-0.290	0.340	0.146	0.198	0.26	0.33	0.41	6.53	2.84
8124.50	-1.688	0.167	-0.511	0.310	0.127	0.154	0.02	0.85	0.13	11.49	1.66
8125.17	-0.495	0.347	0.077	0.170	0.289	0.106	0.76	0.18	0.06	11.78	2.56
8132.17	-0.587	0.338	-0.037	0.212	0.225	0.136	0.58	0.30	0.11	11.87	2.72
8134.20	-1.647	0.227	-0.410	0.318	-0.072	0.245	0.02	0.81	0.17	12.11	0.38
8138.75	-0.611	0.349	-0.225	0.225	0.055	0.147	0.47	0.39	0.13	10.80	1.09
8141.83	-0.702	0.426	-0.418	0.305	-0.094	0.234	0.19	0.55	0.26	12.11	1.74
8146.50	-0.764	0.369	-0.259	0.218	0.001	0.150	0.32	0.50	0.18	12.38	2.67
8156.58	-1.457	0.152	-0.434	0.279	0.068	0.244	0.04	0.91	0.05	11.59	0.76
8164.50	-1.449	0.132	-0.513	0.190	-0.278	0.116	0.04	0.71	0.25	12.67	15.93
8171.00	-1.560	0.121	-0.531	0.164	-0.323	0.098	0.03	0.70	0.27	13.23	14.97
8181.17	-0.865	0.323	-0.386	0.191	-0.150	0.118	0.22	0.57	0.21	12.40	11.88
8184.46	-0.732	0.321	-0.382	0.194	-0.142	0.123	0.27	0.52	0.21	12.22	5.26
8200.08	-0.719	0.327	-0.244	0.171	-0.033	0.103	0.26	0.52	0.22	12.87	9.58
8208.17	-1.476	0.133	-0.671	0.223	0.144	0.165	0.02	0.21	0.77	14.75	52.21
8213.25	-1.470	0.091	-0.512	0.229	0.296	0.070	0.02	0.96	0.02	12.66	6.64
8226.33	-0.464	0.351	-0.069	0.188	0.164	0.117	0.65	0.24	0.11	12.88	4.42
8236.42	-0.793	0.327	-0.181	0.187	0.050	0.116	0.33	0.47	0.19	11.87	6.36
8250.80	-1.434	0.147	-0.402	0.278	0.198	0.215	0.04	0.81	0.15	12.38	5.49
8254.92	-0.601	0.362	-0.194	0.216	0.075	0.133	0.43	0.40	0.17	12.05	4.34
8256.00	-0.723	0.391	-0.084	0.185	0.140	0.115	0.37	0.44	0.20	11.90	6.55
8256.50	-0.659	0.374	-0.169	0.207	0.086	0.130	0.39	0.44	0.17	11.70	3.17
8257.00	-0.691	0.399	-0.163	0.204	0.088	0.126	0.38	0.44	0.18	12.09	5.25
8258.50	-1.346	0.111	-0.505	0.188	-0.226	0.173	0.04	0.56	0.40	12.99	10.59
8282.00	-1.978	0.801	-0.626	0.442	0.096	0.188	0.02	0.27	0.71	12.15	27.35
8312.00	-1.482	0.095	-0.454	0.211	0.062	0.251	0.03	0.97	0.00	12.69	29.06
8319.00	-1.227	0.404	-0.428	0.231	-0.139	0.150	0.05	0.67	0.28	13.21	6.98
8358.58	-1.576	0.084	-0.530	0.191	0.068	0.252	0.03	0.97	0.00	12.24	23.78
8371.50	-1.489	0.106	-0.438	0.193	0.063	0.253	0.02	0.98	0.00	13.28	75.56

Depth *feet*	Avg.1 $log(T_2)$	Std. Dev.1 $log(T_2)$	Avg.2 $log(T_2)$	Std. Dev.2 $log(T_2)$	Avg.3 $log(T_2)$	Std. Dev.3 $log(T_2)$	Weight 1	Weight 2	Weight 3	Multiplier	SSE
8385.50	-1.769	0.106	-0.514	0.176	0.068	0.249	0.02	0.98	0.00	12.61	71.56
8396.50	-1.555	0.061	-0.492	0.151	0.067	0.247	0.01	0.99	0.00	13.43	97.09
8447.70	-1.758	0.076	-0.621	0.139	0.081	0.248	0.01	0.99	0.00	12.09	96.56
8454.25	-1.076	0.151	-0.784	0.194	0.123	0.128	0.29	0.66	0.04	6.95	2.40
8461.80	-1.841	0.131	-0.535	0.270	-0.050	0.281	0.01	0.75	0.23	12.42	2.74
8462.67	-1.398	0.154	-0.425	0.278	0.240	0.189	0.06	0.78	0.16	10.98	3.52
8476.00	-1.557	0.061	-0.677	0.144	-0.469	0.103	0.01	0.68	0.31	11.78	23.52
8488.50	-1.680	0.218	-0.611	0.357	0.152	0.178	0.03	0.53	0.44	9.70	6.05
8499.40	-0.654	0.150	-0.483	0.238	0.108	0.158	1.00	0.00	0.00	12.25	70.53
8522.50	-1.482	0.116	-0.731	0.153	-0.731	0.311	0.00	1.00	0.00	12.54	68.06
8538.00	-0.677	0.186	0.122	0.063	0.122	0.014	0.95	0.05	0.00	10.73	25.43
8551.20	-0.975	0.149	-0.683	0.229	-0.344	0.298	0.10	0.47	0.43	8.53	2.67
8555.20	-0.535	0.357	-0.224	0.291	-0.224	0.281	0.68	0.32	0.00	7.92	0.66
8604.25	-1.054	0.457	-0.165	0.243	0.128	0.165	0.40	0.46	0.15	5.87	0.42
8604.92	-0.937	0.475	-0.356	0.237	-0.065	0.142	0.44	0.37	0.18	7.56	1.79
8608.67	-1.732	0.230	-0.813	0.456	-0.005	0.172	0.04	0.82	0.14	5.22	0.42
8614.67	-0.896	0.323	-0.426	0.289	-0.075	0.220	0.28	0.56	0.16	8.78	0.38
8620.50	-1.774	0.097	-0.597	0.277	0.078	0.095	0.01	0.96	0.03	10.37	1.42
8622.40	-0.660	0.357	-0.022	0.190	0.208	0.119	0.47	0.38	0.15	11.00	3.37
8623.67	-0.910	0.151	-0.639	0.230	0.087	0.156	0.19	0.63	0.18	10.36	3.96
8625.25	-0.687	0.355	-0.012	0.190	0.218	0.120	0.42	0.42	0.16	9.51	2.01
8628.17	-0.643	0.226	-0.643	0.226	0.149	0.071	0.63	0.33	0.04	7.90	5.85
8635.10	-0.515	0.289	-0.234	0.224	0.032	0.154	0.51	0.40	0.09	10.14	3.07
8639.20	-0.901	0.316	0.049	0.192	0.277	0.122	0.30	0.51	0.18	8.79	2.43
8645.70	-0.744	0.298	-0.085	0.218	0.181	0.140	0.37	0.44	0.19	11.91	6.01
8651.33	-1.639	0.100	-0.530	0.294	0.250	0.113	0.01	0.97	0.02	10.94	0.27
8657.50	-0.508	0.284	-0.311	0.202	0.163	0.010	0.89	0.11	0.00	10.88	3.17
8659.80	-1.637	0.157	-0.588	0.244	0.290	0.060	0.03	0.96	0.01	8.98	7.23
8663.70	-0.730	0.391	-0.020	0.205	0.229	0.132	0.70	0.21	0.08	6.78	0.62
8664.50	-1.802	0.010	-0.507	0.257	-0.124	0.182	0.01	0.92	0.07	10.51	6.97
8727.00	-1.465	0.161	-0.807	0.113	0.062	0.104	0.00	1.00	0.00	11.72	96.61
8745.50	-1.464	0.176	-0.831	0.157	0.086	0.132	0.00	1.00	0.00	11.31	42.29
8760.70	-1.195	0.206	-1.195	16.191	-0.139	0.055	0.52	0.45	0.02	7.35	7.66

APPENDIX E

R^2 values for T_2 modeling, all runs.

Depth *feet*	Run 1	Run 2	Run 3
8112.08	0.99622144	0.99889247	0.99926231
8114.7	0.97332202	0.99563693	0.99781112
8116.42	0.98279605	0.9965431	0.99902733
8121.5	0.85551055	0.97784149	0.99133146
8124.5	0.97766654	0.99765703	0.99883699
8125.17	0.96616261	0.99647055	0.99794442
8132.17	0.9554508	0.99527356	0.99783238
8134.2	0.99874262	0.99923702	0.99979001
8138.75	0.97467998	0.99670431	0.99916917
8141.83	0.99281282	0.99851163	0.99895078
8146.5	0.94985432	0.99539943	0.99853245
8156.58	0.99494912	0.99893864	0.9995882
8164.5	0.98232427	0.99284358	0.99526984
8171	0.9814664	0.99528456	0.99667022
8181.17	0.95778528	0.98705828	0.9951459
8184.46	0.96815814	0.99227348	0.99781341
8200.08	0.94164547	0.98526085	0.99663704
8208.17	0.92360673	0.98570548	0.98654477
8213.25	0.99552436	0.99709501	0.99783546
8226.33	0.96216248	0.99414167	0.9975025
8236.42	0.87987782	0.98731759	0.99634566
8250.8	0.9769223	0.99032392	0.99675083
8254.92	0.95170469	0.99161059	0.99737754
8256	0.862935	0.98571174	0.99602071
8256.5	0.93074993	0.99194395	0.99799786
8257	0.91126435	0.98835408	0.99684266
8258.5	0.98994812	0.99482338	0.99651895
8282	0.93597209	0.98694209	0.98713278
8312	0.98936275	0.99155017	0.99155017
8319	0.98555949	0.99620671	0.99757808
8358.58	0.99147863	0.99341036	0.99341036
8371.5	0.98129073	0.98239957	0.98239957
8385.5	0.98289157	0.98360523	0.98360523

Depth *feet*	Run 1	Run 2	Run 3
8396.5	0.98331077	0.98331077	0.98374597
8447.7	0.98123808	0.98123808	0.9816801
8454.25	0.9892629	0.99360388	0.9972846
8461.8	0.98960771	0.99791779	0.99856844
8462.67	0.95642505	0.98448453	0.99710471
8476	0.98709052	0.99356323	0.99406032
8488.5	0.78747994	0.99012688	0.99227238
8499.4	0.98622633	0.98622633	0.98622633
8522.5	0.98699364	0.98699364	0.98697851
8538	0.98062077	0.99074244	0.99074244
8551.2	0.9893507	0.99586613	0.99711808
8555.2	0.99778138	0.99906001	0.99906001
8604.25	0.80955695	0.99437602	0.99826274
8604.92	0.89294517	0.98541095	0.99638568
8608.67	0.96841128	0.99577553	0.99758399
8614.67	0.99174229	0.99911427	0.99950781
8620.5	0.99659602	0.9987965	0.99913302
8622.4	0.84768798	0.99044584	0.99710183
8623.67	0.90703144	0.99223016	0.99713369
8625.25	0.82413185	0.99094005	0.99778201
8628.17	0.98838369	0.99094005	0.99514192
8635.1	0.99402343	0.99740342	0.99781274
8639.2	0.84633168	0.98945461	0.99721784
8645.7	0.86480144	0.98897652	0.99555354
8651.33	0.99826353	0.99918695	0.99984033
8657.5	0.99786934	0.99829186	0.998289
8659.8	0.99277182	0.99324647	0.99490069
8663.7	0.94017902	0.99580876	0.99805399
8664.5	0.99544935	0.99544935	0.99607743
8727	0.98502142	0.98505542	0.98505275
8745.5	0.9898043	0.9898043	0.989822
8760.7	0.9684558	0.97171495	0.97829744

VITA

Domenico Lodola

248 rue de la Crapaudière

37210 Noizay – France

D.E.A., Geology, Université Joseph Fourier, Grenoble 1 (France),

June 2002;

Maîtrise, General Earth Sciences, Université Joseph Fourier, Grenoble 1 (France),

June 2001